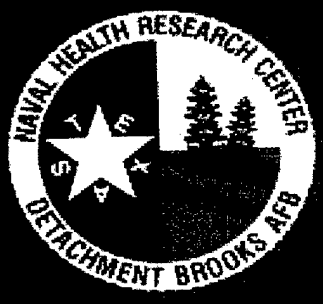

ASSESSMENT OF POTENTIAL RADIATION HAZARD FROM THE COMWIN VEST ANTENNA

John M. Ziriax[1], William Hurt[2], Duane Cox[1], Donald Marchello[1] and John D'Andrea[1]

[1]Naval Health Research Center Detachment
Directed Energy Bioeffects Laboratory
Brooks City-Base, Texas

Technical Report NHRC-DET-DEBL-TR-2003-01

[2]Air Force Research Laboratory
Human Effectiveness Directorate
Directed Energy Bioeffects Division
Radiofrequency Radiation Branch

Technical Report AFRL-HE-BR-TR-2003-0132

Reviewed and approved 2 OCT 2003
Date

Vincent DeInnocentiis, CDR, MSC USN

NOTICES

When U.S. Government drawings, specifications, or other data are used for any purpose other than in connection with a definitely Government-related procurement, the United States Government incurs no responsibility or any obligation whatsoever. The fact that the government may have formulated or in any way supplied the said drawings, specifications, or other data, is not to be regarded by implication, or otherwise in any manner construed, as licensing the holder or any other person or corporation; or as conveying any rights or permission to manufacture, use, or sell any patented invention that may in any way to related thereto.

The views, opinions and/or finding contained in this report are those of the authors and should not be construed as an official Department of the Army, Navy, Air Force and Defense position, policy or decision unless so designated by other documentation.

Trade names of materials and/or products of commercial or nongovernmental organizations are cited as needed for precision. These citations do not constitute official endorsement or approval of the use of such commercial materials and/or products.

This work was supported by SPAWAR, Department of the Navy under Expeditionary Warfare Division of the Office of Naval Research (ONR 353) by the SSC San Diego Signal Procession and Communication Technology Branch (Code 2855) and by the US Army CERDEC Space and Terrestrial Communications Directorate, Antennas and Ancillaries Branch. The views expressed in this article are those of the authors and do not reflect the official policy or position of the Department of the Navy, Department of Defense, or the U. S. Government. Approved for public release; distribution is unlimited.

REPORT DOCUMENTATION PAGE

Form Approved
OMB No. 0704-0188

1. REPORT DATE *(DD-MM-YYYY)*	2. REPORT DATE	3. DATES COVERED *(From - To)*
19-09-2003		Aug 2002- Aug 2003

4. TITLE AND SUBTITLE
ASSESSMENT OF POTENTIAL RADIATION HAZARD FROM THE COMWIN VEST ANTENNA

5a. CONTRACT NUMBER

5b. GRANT NUMBER

5c. PROGRAM ELEMENT NUMBER
06022782

5d. PROJECT NUMBER

5e. TASK NUMBER

5f. WORK UNIT NUMBER
D07072

AUTHOR(S)
John M. Ziriax[1], William Hurt[2], Duane Cox[1], Donald Marchello[1], and John A. D'Andrea[1]. [1]Naval Health Research Center Directed Energy Bioeffects Laboratory, 8315 Navy Road, Brooks City-Base, Texas 78235; [2]Air Force Research Laboratory, Human Effectiveness Directorate, Directed Energy Bioeffects Division, Radiofrequency Radiation Branch, Brooks City-Base, Texas 78235

7. PERFORMING ORGANIZATION NAME(S) AND ADDRESS(ES)
Naval Health Research Center
P.O. Box 85122
San Diego, CA 92186-5122

8. PERFORMING ORGANIZATION REPORT NUMBER
NHRC-DET-DEBL-TR-2003-01
AFRL-HE-BR-TR-2003-0132

9. SPONSORING/MONITORING AGENCY NAME(S) AND ADDRESS(ES)
Office of Naval Research
800 North Quincy St.
Arlington, VA 22217-5600

Space and Naval Warfare Systems Center
53560 Hull Street
San Diego, CA 92152-5001
Washington, DC 20372-5300

10. SPONSOR/MONITOR'S ACRONYM(S)
ONR, SPAWAR

11. SPONSORING/MONITORING AGENCY REPORT NUMBER

12. DISTRIBUTION AVAILABILITY STATEMENT
Approved for public release; distribution is unlimited.

13. SUPPLEMENTARY NOTES

14. ABSTRACT

The COMbat Wear Integration (COMWIN) antenna is currently being developed by Dr. Richard Adams of SPAWAR Systems Center, San Diego (Adams et al., 1999, Adams et al., 2000; Adams et al,. 2001; and Adams et al., 2002). The antenna would replace the whip antenna on man portable radios with a vest partially composed of a conductive fabric. The vest would make it more difficult for adversaries to locate and identify radio operators and would not interfere with operator's movement in the way a protruding antenna would. These advantages result because of the close proximity of the antenna to the body of the operator. This report describes the results of an assessment of the radio frequency energy deposited in the body of the operator wearing three versions of the Mark III COMWIN vest antenna. A human phantom was used for the measurements because probes must be inserted within the body. Local specific absorption rates (SARs) were measured in the homogeneous tissue equivalent phantom using non-perturbing temperature probes at frequencies ranging from 30 to 450 MHz. In addition, local and whole body SARs were calculated using the Brooks anatomical man model. The results of the empirical measurements and the theoretical modeling suggest that, given a net input power to the antenna of 5W, the energy absorbed by the operator would not exceed current safety standards even if the operator were to transmit continuously. Under normal operation, when transmission is interrupted, the duty cycle of the antenna and the resulting SAR will be substantially lower.

15. SUBJECT TERMS
vest antenna, specific absorption rate, induced currents, radiofrequency, high frequency, safety, electromagnetic radiation

16. SECURITY CLASSIFICATION OF:			17. LIMITATION OF ABSTRACT	18. NUMBER OF PAGES	19a. NAME OF RESPONSIBLE PERSON
a. REPORT	b. ABSTRACT	c. THIS PAGE		12	Vincent Deinnocentiis, CDR, MSC USN
Unclassified	Unclassified	Unclassified			19b. TELEPONE NUMBER *(Include area code)* 210-536-6924

CONTENTS

ABSTRACT

The **COM**bat **W**ear **In**tegration (COMWIN) antenna is currently being developed by Dr. Richard Adams of SPAWAR Systems Center, San Diego (Adams et al., 1999, Adams et al., 2000; Adams et al,. 2001; and Adams et al., 2002). The antenna would replace the whip antenna on man portable radios with a vest partially composed of a conductive fabric. The vest would make it more difficult for adversaries to locate and identify radio operators and would not interfere with operator's movement in the way a protruding antenna would. These advantages result because of the close proximity of the antenna to the body of the operator. This report describes the results of an assessment of the radio frequency energy deposited in the body of the operator wearing three versions of the Mark III COMWIN vest antenna. A human phantom was used for the measurements because probes must be inserted within the body. Local specific absorption rates (SARs) were measured in the homogeneous tissue equivalent phantom using non-perturbing temperature probes at frequencies ranging from 30 to 450 MHz. In addition, local and whole body SARs were calculated using the Brooks anatomical man model. The results of the empirical measurements and the theoretical modeling suggest that, given a net input power to the antenna of 5W, the energy absorbed by the operator would not exceed current safety standards even if the operator were to transmit continuously. Under normal operation, when transmission is interrupted, the duty cycle of the antenna and the resulting SAR will be substantially lower.

ACKNOWLEDGMENTS

The authors wish to thank Rich Adams and Wayne Hammer for their careful review of earlier versions of this manuscript.

OVERVIEW

Scientific Approach

In the last three decades, the use of devices that emit radio frequency (RF)[1] fields has increased dramatically. The proliferation of RF devices has been accompanied by increased concern about ensuring the safety of their use. Throughout the world many organizations, both government and non-government, have established RF safety standards or guidelines for exposure. Generally, the guidelines limit the specific absorption rate (SAR) of energy deposited into the human body between 100kHz and 300GHz. Thus, new devices like mobile phones are being evaluated for the amount of RF energy deposited in the human head (Van de Kamer and Lagendijk, 2002). Newer devices that are being developed include antennas for wireless devices, which are incorporated into clothing. The topic of this report is an analysis of an antenna incorporated into a wearable vest and whether this concept meets the current safety guidelines (IEEE C95.1, 1999; DODI 6055.11).

Rate of energy deposition into the operator of the COMWIN antenna was estimated using two independent methodologies. First, local SARs were measured with non-perturbing temperature probes. The probes were located in the areas of a tissue equivalent phantom near the feed of the antenna on the backside and near the shorting strap on the front side. These locations were selected because the highest electrical fields have been measured in these areas, so they were likely to be associated with the highest local SARs. Second, whole body and local SARs were estimated using the Brooks anatomical man model and a finite difference time domain (FDTD) radio frequency (RF) dosimetry program. The use of two independent methodologies provides confirmation of the level of operator exposure.

Thermometry

RF energy absorbed by a lossy material such as tissue produces heat. Measurement of this heating can be difficult and even impossible depending on a variety of conditions. In living tissue, blood flow and thermoregulatory mechanisms tend to spread the thermal energy over a much larger volume. Worse yet, the more energy deposited, the more active these mechanisms become. For this reason, living tissue is rarely used. For animal experiments, carcasses may be used. Obviously, this is not possible when assessing human exposures. A well-established alternative is the use of a non-perturbing waterproof fabric form, filled with tissue equivalent material (TEM) (Chou et al.,

[1] The radio frequency portion of the electromagnetic spectrum extends over a wide range of frequencies, from about 10 kHz to 300 GHz.

1984). The material is a mixture designed to have the same electrical properties as the whole body over a specified frequency range. The use of phantoms composed of TEM eliminates the problems posed by living tissue, with the additional advantage of allowing the easy placement of temperature probes.

Even in a TEM phantom, thermal conduction can still be a problem. Accurate measurement of RF-induced temperature increases requires that the effects of thermal conduction be minimized. This is accomplished in two ways. First, the target is exposed at as high a power as is possible and for as brief a period of time as possible to minimize heat being conducted away from the site of deposition. Second, exposure duration and powers are minimized to limit the heating induced in the phantom to no more that is required for accurate measurement. This accomplishes two goals: First, it allows the phantom to re-equilibrate rapidly, keeps the temperatures in the ideal range of the thermometers. And second, it minimizes the effect of energy deposited adjacent to the measurement locations. Finally, a mathematical method (Gambrill et al., 1993; Lu, et al., 1993) has been devised, which minimizes the effects of thermal instabilities in the phantom by subtracting the pre- and post-exposure rates of temperature change from the rate during exposure.

Theoretical Modeling

The finite difference time domain (FDTD) method is widely used to model RF absorption by a variety of targets including the human body (Shlager and Schneider, 1995; and http://www.fdtd.org). Briefly, the FDTD method, developed by Yee (1961), allows the simultaneous computation of propagation of the electric and magnetic fields. The method has been applied to problems in three dimensions (Kunz and Luebbers, 1993; and Taflove, 1995). In this case, the volume to be modeled is described by a three-dimensional grid. At each location in the grid or voxel, a material or tissue type is identified. Each tissue type has physical and electrical properties associated with it. The FDTD method simulates the propagation of the electrical and magnetic fields associated with an RF exposure through this volume by solving Maxwell's equations at finite increments of time at each voxel location.

The FDTD method, then, requires: (1) a software implementation of the FDTD method, XFDTD (REMCOM, Inc, State College, PA); (2) a frequency-dependent description of the physical electrical properties of the tissues to be modeled, we used data reported by Gabriel et al. (1996); and, finally, (3) an anatomical model, we used the 5-mm version of the Brooks man model (Mason et al., 1998).

METHOD

Equipment

COMWIN Prototype Vest Antennas

Three slightly different versions of prototype Model 3 of the vest antenna were used during the experiment (Adams et al, 1999, Adams et al, 2000; Adams et al, 2001; and Adams et al, 2002). One of the antennas is pictured in Figures 1 and 2. The antenna elements are made of a copper/polyester composite fabric called Flectron 3027-106 (Laird Technologies, Delaware Water Gap, PA 18327, http://www.lairdtech.com) sewn to a canvas shell. Power is input to the antenna through a connector on the back of the antenna (Figure 2). The three versions of the vest antenna tested in these experiments differed only in the amount and type of material inserted into pockets sewn on the inside of the antenna directly behind the two horizontal antenna elements. Vest F had 2 cm thick anechoic material in the pockets. Vest K had an "unmarked" tubular composite material (15% copper tubules and 5% iron powder) acquired from Dr. Paul Schoen (Naval Research Laboratory). And Vest G was the same as Vest F except that the absorber behind the antenna feed was removed.

Transmitters

The vest antennas were tested using two different RF Amplifier sources. The ENI Model A1000 RF amplifier (MKS, ENI® Products, Rochester, NY) provided energy in the 30 to 65 MHz range, and the BHE Series amplifier (Comtech PST Corp., Melville, NY) provided RF in the 70 to 400 MHz range. Both amplifiers were operated outside the recommended frequency range to cover all of the required test requirements. The output of the source was connected to a bidirectional coupler where the attenuated forward and reflected power samples could be measured with a dual input Hewlett Packard 438A power meter (Hewlett Packard, Palo Alto, CA). During the high power tests, an additional 10dB was added to the forward and reflected sample ports to give a total of 30 to 36db depending on what frequency was being used. The power meter provided the net power to the vest by internally taking the difference from the forward to reflected power. The net power was used to normalize the SAR data. Power levels unless otherwise noted, refer to net power.

Tissue Equivalent Phantom

The casing for the phantom was similar to human phantoms used previously in the laboratory (Olsen and Griner, 1989; Olsen, 1982) except that the extremities were truncated at mid upper arm, mid thigh and neck. This modification allowed for easy manipulation of the vest while the phantom was

suspended from the ceiling by a nylon harness. The tissue equivalent material (TEM), prepared according to a recipe for the 100 to 300 MHz frequency range (Chou et al., 1984), was a mixture of aluminum powder, solidifying powder (TX-151), salt, and water that simulates the dielectric and conductive properties of a person in a limited frequency range.

The specific heat for the TEM jell mixture has also been characterized (Leonard et al., 1984) at 3600 J/(kg°C). This value was used to convert rate of temperature increases to specific absorption rate (SAR as W/kg) according to the following formula:

$SAR = 3600[T_{exposed} - T_{control}]/(\text{exposure time in seconds})$

For example, given an initial temperature of 21°C and an ending temperature of 21.4°C following a 60 second exposure yields 24 W/kg. A rule of thumb is a 1°C/min temperature rise is equivalent to an SAR of 60 W/kg.

This basic procedure assumes that the baseline rate of temperature change of the phantom is zero. However, because large phantoms may require hours to equilibrate, this is frequently not the case. Nor would it be desirable to be limited to a single measurement every few hours. A refinement of the basic procedure (Gambrill et al., 1993; Lu, et al., 1993), avoids this problem, and can be used with thermally unstable samples. The refinement takes the baseline rate of temperature change a few minutes before and after each exposure. The average rate of temperature change during these non-exposure periods is subtracted from the rate of change during exposure. The result is the rate of temperature change produced by the exposure. By correcting the rate of temperature change, many more exposures may be performed with no loss of accuracy. In these measurements all pre-exposure, exposure, and post exposure periods were two minutes in duration. Temperature was sampled at each probe once every five seconds.

Non-perturbing Thermometry

Temperature measurements were performed using FISO fiber-optic temperature sensor system (UMI, FISO Technologies Inc., Saint-Foy, Canada, http://www.fiso.com). The probe locations are listed in Table 1 to 5. Temperature data were collected for two minutes prior to the application of input power, during the two-minute application of RF power to the antenna, and for an additional two minutes after RF power was terminated. The pre- and post-RF exposure temperature data established the baseline thermal profile at each probe location allowing the thermal data collected during RF exposure to be corrected for ongoing changes in temperature not directly related to the RF exposure.

Infrared Video Camera

An infrared video camera (Radiance 1 from Amber-Raytheon, Goleta, Georgia) was used to record temperature changes on the exterior surface of the

vest antenna as power was applied. These changes were a concern because power applied was far in excess of the design specifications of the antenna. The high power levels were required to produce reliably detectable temperature changes in the TEM phantom.

Data collection procedure

The phantom was suspended in a harness so that its shoulder was 1.5 m above the floor. The vest was placed on the phantom such that the arms of the phantom were inside the vest. This was done because, in this configuration, measurements of the voltage standing wave ratio (VSWR) of the phantom most closely matched previous VSWR measurements made with several humans wearing the vest (Adams et al, 1999, Adams et al, 2000; Adams et al, 2001; and Adams et al, 2002). It appeared that the improvement was a result of the arms bringing the vest into closer proximity of the phantom's torso. The antenna was then connected to the transmitter and two-minute baseline temperature measurements started. At the end of this period, RF power at the selected frequency was applied to the vest for two minutes. Forward and reflected power were monitored to insure that net power transmitted by the vest remained at the desired level throughout the exposure. Immediately after the RF power was turned off the two-minute post-exposure measurements were started.

RESULTS

Thermometry

Tables 1 through 5 list the temperature probe locations, frequencies, input powers, SARs normalized to 1-W input power and SARs normalized to a 5-W input power. Tables 1 to 3 list the results for Vest F, and Tables 4 and 5 list the results for Vests G and K, respectively. In all five tables, each row is the result for a single temperature probe on a single run.

The first five columns of the table identify, the run and the probe location. The first column of the tables indicates the file reference number, and the second column is a "B" if the probe was inserted from the back of the phantom and an "F" if the probe was inserted from the front. The next column describes the location of the insertion point or "Position". Position is described as -1, 0, 1, or 2. Since all probes were inserted on the midline of the vest and phantom, the position number indicated vertical location along the midline. On the front the zero position was half way between the horizontal FLECTRON antenna straps and just to the right of the vertical shorting strap (See Figure 1). The other positions were position above or below the zero position either 2.5 cm, for position -1 and 1, or above 5 cm for position 2. Similarly, on the backside (See Figure 2), the zero position was also midway between the two large horizontal straps, with the other positions above or below that by 2.5 or 5 cm. The next column shows the depth of the probe as measured from the surface of the phantom in centimeters.

The sixth column of the table lists the frequency of the run in megahertz (MHz), with the next column indication the Run Number. When a set of conditions was repeated, the Run Number was incremented. Finally, the last three columns show the net power in Watts (input minus reflected power); the Measure SAR normalized to 1 W of net input power (W/kg/W); and finally, the SAR normalized to a 5 W net power (W/kg/5 W).

Since the expected operating power of the antenna is 5 W and the localized exposure limit is 8 W/kg (DOD I 6055.11; IEEE C95.1-1999; OPNAVINST 5100.23F), it is significant that the maximum observed localized SAR was 3.67 W/kg/5W on the back at Position 1 at a depth of 0.5 cm during run number 2 at 225 MHz (See Table 2 the eighth row). This value is less than half of the standard assuming continuous transmission for 6 minutes. A run under the same conditions using Vest G is shown on the thirteenth row of Table 4. The modifications to the vest reduced the 5 W normalized SAR by a factor of 10 to 0.34 W/kg/5W. An examination of the data for Vests G and K show a maximum localized SAR of 1.98 W/kg/5W at Back Position 0 at a depth of 0.5 cm and 275 MHz (Row 3 of Table 4). This value is approximately 25% of the maximum

allowed by the standard. A graphical analysis of the thermometric data is presented in Figures 3 to 31 with the analysis of the FDTD results.

Infrared Video Recordings

Infrared video recordings were used to monitor the temperature changes on the visible exterior surfaces of the phantom and vests. When 200 W was initially input to the vest antenna, a great deal of heat was generated at the shorting strap. Smoke appeared. By the time the power was shut off, the strap and canvas backing had burned through. Copper tape was used to replace the FLECTRON cloth in the shorting strap to good effect. Because of the ohmic heating in this area of the vest, the infrared camera was focused on the front of the vest throughout the remainder of the tests.

Sample infrared images are shown in Figures 33 to 35. The images highlight one of the difficulties with performing this sort of experiment. In order to reliably measure RF-induced heating in the phantom, much more than the rated power was put into the vests. This is good, in the sense that the vests were not efficiently heating the phantoms, but it presents a second source of heat, which is an artifact of the high powers used. Thus, the implanted temperature probes may have measured heat from the over-powered vest, an artifact, in addition to the RF heating of interest. Since heat from the vest would be external to the phantom, temperature probes positioned nearer the surface would be more likely to be affected. In any case, the "extra" heat from the over-powered vest means that the SARs will tend to overestimate the operator's actual exposure.

Modeling Results

FDTD data for the areas where the temperature probes were located are presented in Tables 6 to 9, in graphs in Figures 3 to 14, and as images in Figures 16 to 31. The tables present the SARs calculated by the FDTD at each Position by depth in 5 mm increments and by frequency. Table 6 through 9 presents the results at Position 2, 1, 0 and -1, respectively. The same data are presented as graphs in figures 3 through 14. Each graph plots SAR as a function of depth from the back ending at the front surface. Each curve represents a single frequency as listed in the key of each graph. Finally, where applicable, SAR data from all of the implanted temperature probes are plotted as larger unconnected symbols.

A similar pattern is seen in all graphs. First, a peak at depths from 10 to 45 mm is observed at all frequencies and locations. The height and exact shape varies with frequency and location. At Position 2 the height of the peak declines from 30 MHz to 90 MHz (Figures 3 and 4), reaches its highest measured value at 225 MHz (SAR 0.169 W/kg/W) before declining again up to 450 MHz. A similar peak is observed at Position 1 (peak SAR at 225 MHz is 0.23 W/kg/W),

Position 0 (peak SAR at 225 MHz is 0.28 W/kg/W), and Position -1 (peak SAR at 225 MHz is 0.264 W/kg/W).

Higher SARs near the back surface occurred at Positions 0 and -1 at all frequencies (Figures 9 to 14) and to lesser extent at Position 1 at the higher frequencies, 225-450 MHz (Figure 8). Much smaller peaks are observed at Positions 2, 1, and 0 at depths of 120 to 130 mm and 230 to 250 mm (Figures 3 to 11).

Comparisons of FDTD results with empirical measurements are possible in Figures 5 to 13. A detailed description of Figure 5 will serve to illustrate the remaining Figures of this type. As before the FDTD data is plotted as a series of lines connecting smaller symbols. Each line represents the calculated SAR at a single frequency, listed in the key, and at a series of depths measured from the back surface of the model through to the front surface. Obviously, the length of this line will vary depending upon the anatomical location. The thermal data is plotted with larger colored symbols. The color of the symbol is either blue, if the data was collected with Vest F or red for Vests G or K (only one of these two is plotted on any graph). The key lists the frequency followed by the Vest letter designation and if a run was replicated the number of the replication. For example, in Figure 5 the inverted red triangle is labeled "275 MHz – G 2" in the key. This indicates that data with this symbol was collected at 275 MHz using Vest G and that this was the second run under these conditions. In Figure 5, all of the thermal data were collected at a depth of 5 mm from Vest F, the blue symbols, or Vest G, the red symbols. Because not all of the thermal data points would fit on the scale used to plot the FDTD data, as insert of the first 30 mm is shown to the left of the key. The expanded scale of this and all other inserts ranges from 0 to 0.8 $W/kg/W_{input}$ instead of the 0 to 0.35 $W/kg/W_{input}$ of the larger figures.

In comparing the FDTD and empirical data shown in Figure 5 and the other similar figures, it is important to remember that the thermal data (colored points) were collected with a homogeneous phantom at input power levels which produced ohmic heating in the vest (See Figures 33-35). Therefore, any comparison of the two data sources must consider that the thermal data collected near the phantom surface may be contaminated by ohmic heating from the vest as opposed to direct microwave heating of the tissue equivalent material. This source of error will cause the temperature-based data to overestimate the SAR relative to the FDTD. And indeed, the thermal measure of SAR is either at or above the FDTD values. A second feature is the appearance of well-defined peaks in the FDTD data. These correspond to changes in tissue type along the line through the model. Since the electrical properties of TEM are the average of those of the body, it is reasonable to expect that the SAR measured in TEM should approximate that predicted by the heterogeneous FDTD results. Generally speaking, this appears to be the case as well. Unfortunately, infrared images were not collected for the front and back of the

vest at the end of every run. This makes it impossible to correlate heating observed with infrared camera with heating observed by the implanted temperature probes.

Table 10 summarizes the FDTD results normalized to a 5 W net input power for each of the frequencies listed in the first column of the table. Subsequent columns show the maximum SAR using an averaging volume of 0.125 g (1/8 g, this mass approximates a single 5 mm by 5 mm by 5mm voxel), 1 g, and 10 g. The whole body average (WBA) SAR is listed in the fifth column of the table. The last column shows the input impedance of the antenna at each of the frequencies. The maximum WBA SAR occurs at 30 MHz with 0.051 W/kg. Using 1 and 10 g averaging volumes, the maximum SARs also occur at 30 MHz with a SAR of 6.5 W/kg and 2.4 W/kg, respectively. A 0.125 g or single voxel maximum SAR occurs at 325 MHz with a SAR of 8.5 W/kg, though 30 MHz is second highest with 7.8 W/kg.

DISCUSSION

The purpose of this project was to make a best effort at determining the localized SARs experienced by a radio operator wearing a Mark 3 COMWIN vest antenna. A secondary goal was to develop techniques for estimating these SARs both empirically with thermometry and theoretically using FDTD modeling. As future versions of the COMWIN antenna are developed, it is hoped that better estimates will be possible.

Exposure standards

As a device designed for use in close proximity to the human body, it is essential that the COMWIN antenna conform to safety standards (DOD I 6055.11 and IEEE C95.1-1999). As any user of the COMWIN antenna will be well informed as to the potential risks and mitigating factors applicable to its use, the antenna can be considered a controlled environment. The standard for a controlled environment include a factor-of-10 safety margin below the minimal effect level. The effect is an acute behavioral response, work stoppage, observed in rats and rhesus monkeys working for food (D'Andrea, 1977; deLorge, 1983). No long-term health effects were reported following these exposures. As such, the standards are conservative, in that the effect protected against has no known long-term health consequences. The standards limit the 6-minute average SAR to a WBA SAR of 0.4 W/kg and a 1-g average SAR of 8 W/kg.

Ohmic Heating vs. RF-induced Heating

A possible confound in this study is the heating of the vest itself resulting from the high input powers used. The vest was designed for an input power of 5 Watts. However, in order to produce rapid detectable heating in the phantom, powers as high as 200 Watts were used. It is not surprising that these high power levels produced resistive heating in the Flextron fabric of the vest. This thermal energy could have contaminated the temperature data collected by the probes located near the surface of the phantom. An examination of the infrared images in Figures 33 to 35 shows that vest heating was frequency related, with lower frequencies, 30 and 55 MHz, producing more vest heating. In all cases the greatest heating was not located on the midline of the phantom where the temperature probes were inserted; however, given the small temperature changes being measured within the phantom, the vest heating along the midline could still have confounded these measurements. That said, the measured temperatures when transformed into SARs are still well below the safety standard for a 1-gram average volume of 8 W/kg. The maximum measured local SAR 3.67 W/kg/5 W on the back at Position 1 at a depth of 0.5 cm during run number 2 at 225 MHz (See Table 2 the eighth row) is less than half the

safety standard assuming no thermal contamination from vest heating and continuous transmission for 6 minute.

Theoretical Modeling

The second source of information on the exposure of the wearer of the COMWIN antenna is the FDTD model. FDTD is widely used to calculate RF exposures using realistic models of inanimate objects and biological systems as well. The advantage of the finite difference methods is that it allows a much greater level of detail to be modeled than say finite element or method of moments approaches. This is a particularly important advantage when the system of interest is a complex biological system such as the human body.

Anatomically Realistic Human Model

Even though the empirical measurements were made using a homogeneous phantom, the FDTD calculations reported above used a heterogeneous human model. This was done because the system of interest is the human body and the FDTD results using the realistic anatomical model provides an intermediate between the empirical results using the phantom and the eventual human users of the vest antenna. An examination of Figures 3-14 show changes in SAR as a function of depth which correspond to changes in anatomical tissue type. This point is also illustrated by the comparisons of the image of the anatomical model in Figure 15 to the SAR distributions shown in Figures 16 to 31.

FDTD Results: Whole Body Average SAR

In this study, whole body average SAR could only be estimated from the FDTD results. Based on these results, the WBA SAR given a 5 W net input to the COMWIN antenna and continuous transmission for 6 minutes, yields a maximum of 0.051 W/kg or roughly $1/8^{th}$ of the standard. Assuming a 6-minute conversation with the vest wearer transmitting 50% of the time, the WBA SAR would be 0.026 W/kg or roughly $1/16^{th}$ of the standard.

The correspondence between the trends and values seen in the measured SAR values (higher SARs towards the back) and those predicted by the model suggests that, in spite of the large differences between the two methods, there is overall agreement. Clearly, if the goal had been to validate the two methods two changes would be required. First, many more temperature probes would be required to map the SAR distributions in the phantom. This rapidly becomes impractical as the number of probes rises. And second, the FDTD could be run using the same electrical properties for all tissue types. That, however, was not the goal. Rather, using the existing empirical data as samples and recognizing that the anatomical model tended to shift RF absorption from the surface and fat tissues to the muscle tissues, it is clear that the SAR

absorption experienced by humans is approximated by both methods, and that the rate of absorption is substantially less than the whole body and localized 1g SAR standards.

REFERENCES

Adams, R. C., C. P. Haglind, H. Pace, J. Lebaric, R. Adler, T. M. Gainor, and A. T. Tan, "Fiscal Year 1999 Wideband Antenna Feasibility study: Man-Carried Ultra Wideband Antenna System." 1999. Technical Report 1808 (Nov). SAWAR Systems Center, San Diego, CA.

Adams, R. C., R. S. Abramo, J. L. Parra, and J. F. Moore. 2000. "COMWIN Antenna system Fiscal Year 2000 Report." Technical Report 1836 (Sep). SPAWAR Systems Center, San Diego, CA.

Adams, R. C., R. S. Abramo, and D. W. Von Mueller. 2001. "COMWIN Antenna Project: Fiscal Year 2001 Final Report." Technical Report 1866 (Aug). SPAWAR Systems Center, San Diego, CA.

Adams, R.C., D. W. Von Mueller. 2002. "COMWIN Antenna Project: Final Report FY 1999 to 2002." Technical Report 1892 (Sep). SPAWAR Systems Center, San Diego, CA.

Chou C. K., Bassen H., Osepchuk J., Balzano Q., Petersen R., Meltz M., Cleveland R., Lin J. C., Heynick L. "Radio frequency electromagnetic exposure: tutorial review on experimental dosimetry." *Bioelectromagnetics.* 1996;*17*(3):195-208.

Chou, C. K., G. W. Chen, A. W. Guy, and K. H. Luk, "Formulas for Preparing Phantom Muscle Tissue at Various Radiofrequencies," *Bioelectromagnetics*, 1984, *5*, 435-441.

D'Andrea JA, Gandhi OP, Lords JL. Behavioral and thermal effects of microwave radiation at resonant and non-resonant wavelengths. *Radio Science*, 1977, *12*, 251-256.

de Lorge JD. 1983. The thermal basis for disruption of operant behavior by microwaves in three animal species. In Adair ER (ed.) *Microwaves and thermoregulation.* New York: Academic Press, pp. 379 - 399.

Department of Defense. 1995. "PEL (Permissible Exposure Limits) for Controlled Environments." DODI 6055.11 (Feburary 21).

Department of the Navy. 2002. OPNAVINST 5100.23F (15 Jul). "Non-Ionizing Radiation," Chapter 22 in *Navy Occupation and Health Program Manual,* Washington, D.C.

Durney, C.H.; Johnson, C.C.; Barber, P.W.; Massoudi, H.; Iskander, M.F.;

Lords, J.L.; Ryser, D.K.; Allen, S.J.; Mitchell, J.C. *Radiofrequency radiation dosimetry handbook.* SAM-TR-78-22, Brooks Air Force Base, San Antonio, TX, 1978.

Gabriel C. *Compilation of the Dielectric Properties of Body Tissue at RF and Microwave Frequencies*, Brooks AFB, TX: Armstrong Laboratory Report, AL/OE-TR-1996-0037, 1996.

Gambrill, C.S. DeAngelis M.L., Lu S-T. Error analysis of a thermometric microwave-dosimetry procedure. In: Blank M, editor. *Electricity and magnetism in biology and medicine*, San Francisco: San Francisco Process. 1993. 593-595.

IEEE/ANSI C95.1. Institute of Electrical and Electronics Engineers (1999): *IEEE/ANSI Standard for Safety Levels with Respect to Human Exposure to Radio Frequency Electromagnetic Fields, 3 kHz to 300 GHz*, New York, NY.

Kunz, KS and Luebbers RJ. *"The Finite Difference Time Domain Method for Electromagnetics"*, CRC Press, Inc., Boca Raton, FL, 1993.

Leonard, N. B., K. R. Foster, and T. W. Athey. "Thermal Properties of Tissue Equivalent Phantom Materials," *IEEE Transactions on Biomedical Engineering*, Vol. BME-31, No. 7, July 1984, 533-536.

Lu S-T, DeAngelis ML, Gambrill CS. Ocular microwave thermometric dosimetry and thermometry in the rabbit. In: Blank M, editor. *Electricity and magnetism in biology and medicine.* San Francisco: San Francisco Press, Inc. 675-678; 1993.

Mason PM, Ziriax JM, Hurt WD, D'Andrea JA. 3-Dimensional models for EMF dosimetry. In *Electricity and Magnetism in Biology and Medicine* edited by Bersani, Kluwer Academic/Plenum Publishers, 1999.

Mason PM, Walters TJ, Fanton JW, Erwin DN, Gao JH, Roby JW, Lott KA, Lott LE, Blystone RV. Database created from magnetic resonance images of a Sprague-Dawley rat, rhesus monkey, and pygmy goat. *FASEB J.*, 9:434-440, 1995.

Olsen, R. G. "Far-Field Dosimetric Measurements in a Full-Sized Man Model at 2.0 GHz," *Bioelectromagnetics*, Vol. 3, p. 433, 1982.

Olsen, R.G. and T.A. Griner. 1989. Outdoor Measurement of SAR in a Full-Sized Human Model Exposed to 29.9 MHz in the Near Field, *Bioelectromagnetics*, vol. 10, pp. 161-171.

Shlager, K.L. and Schneider, J.B., **A** Selective Survey of the Finite-Difference Time-Domain Literature. *IEEE Antennas and Propagation Magazine*, 37:4, pp. 39-56, 1995.

Taflove, A. 1995. *Computational Electrodynamics: The finite-Difference, Time-Domain Method*, Artech House, Norwood, MA.

Van de Kamer JB, and Lagendijk, JJW. Computation of high-resolution SAR distributions in a head due to a radiating dipole antenna representing a hand-held mobile phone. Phys. Med. Biol. 47 (21 May 2002) 1827-1835.

Yee, K.S., Numerical solution of initial boundary value problems involving Maxwell's equations in isotropic media. *IEEE Transactions on Antennas and Propagation*, Vol. 14, p. 302, 1966.

LIST OF FIGURES

Figure 1. Front view of COMWIN vest antenna worn by developer, Dr. Rich Adams.

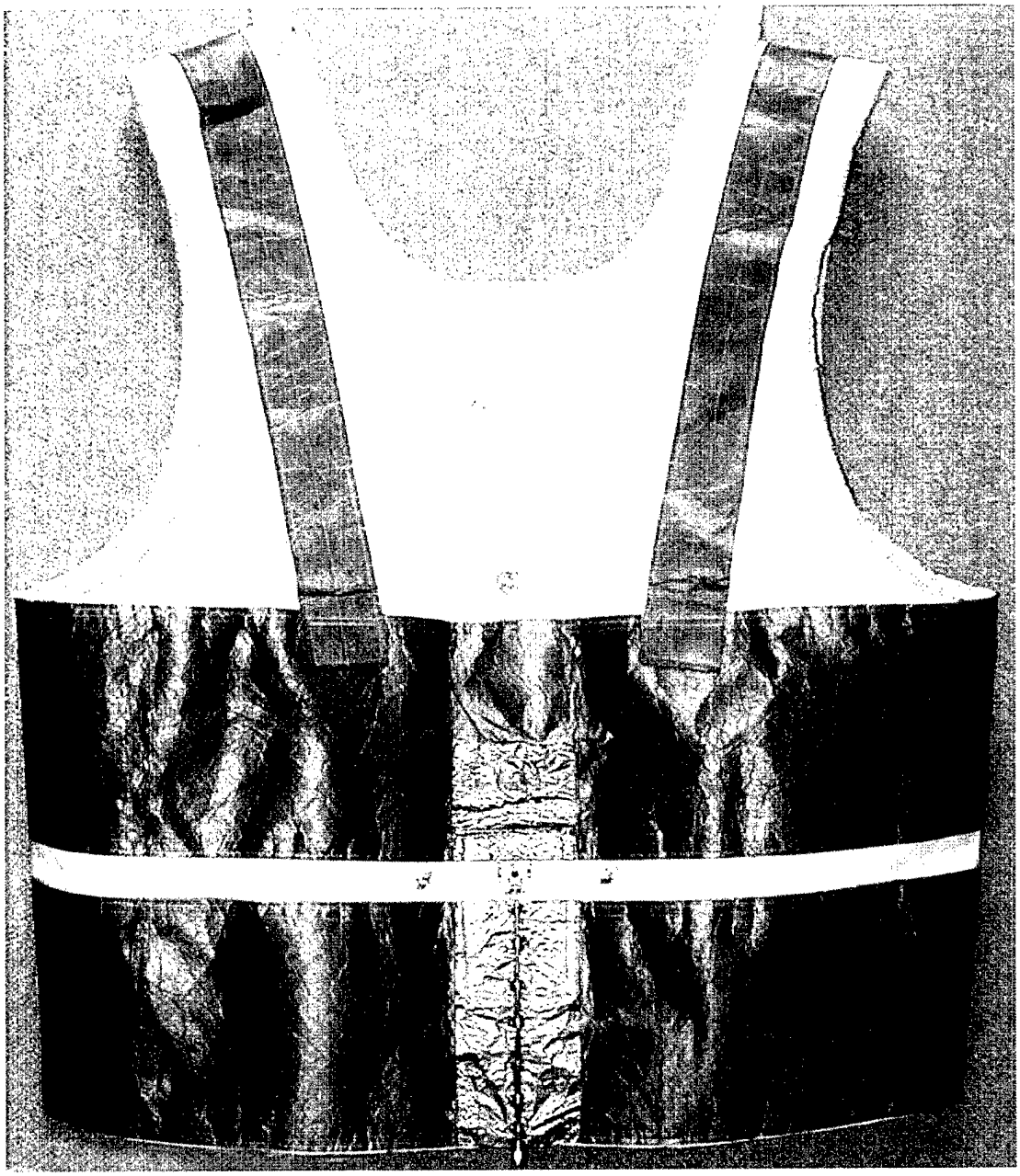

Figure 2. Rear view of vest antenna. Probe locations are mapped along the vertical mid-line of the vest from Position 0 midway between the two large horizontal straps. Position 1 is up 2.5 cm, and Position 2 is up 5 cm from Position 0. Position -1 is down 2.54 cm from Position 0. Probe depths were measured from the surface of the phantom at the point of insertion.

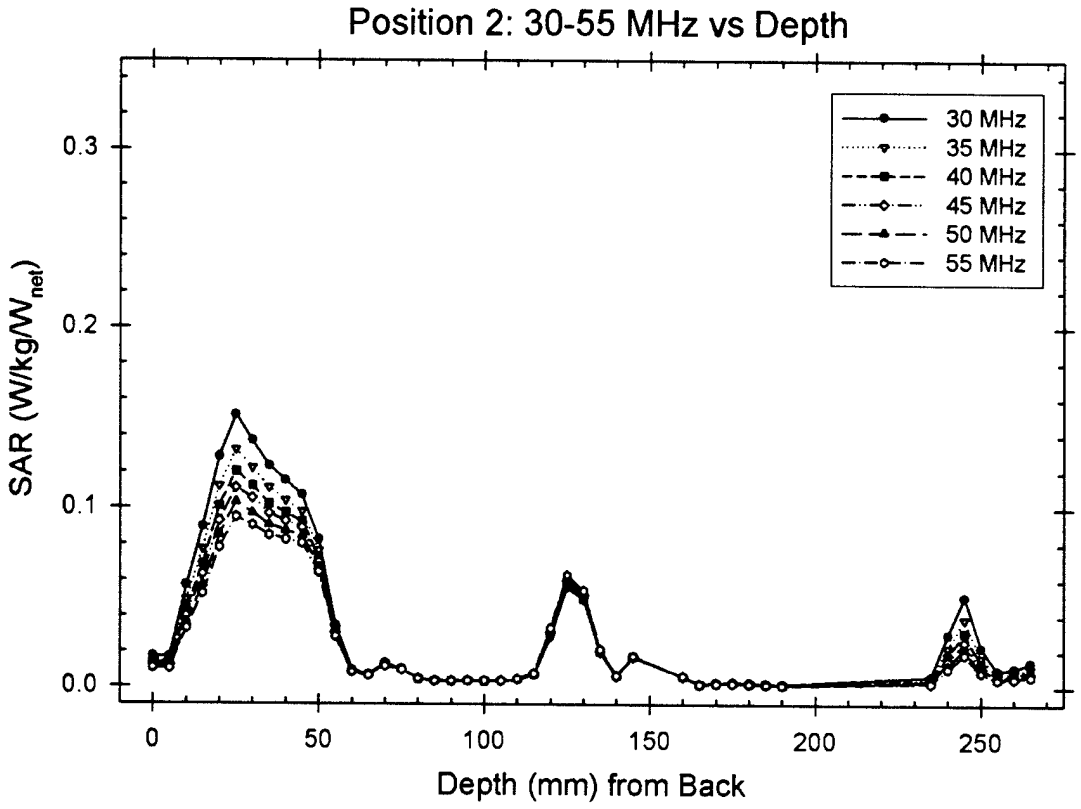

Figure 3. FDTD results (black lines) at Position 2. SAR versus depth as measured from the back surface of the anatomical model for frequencies 30, 35, 40, 45 50 and 55MHz (black symbols)

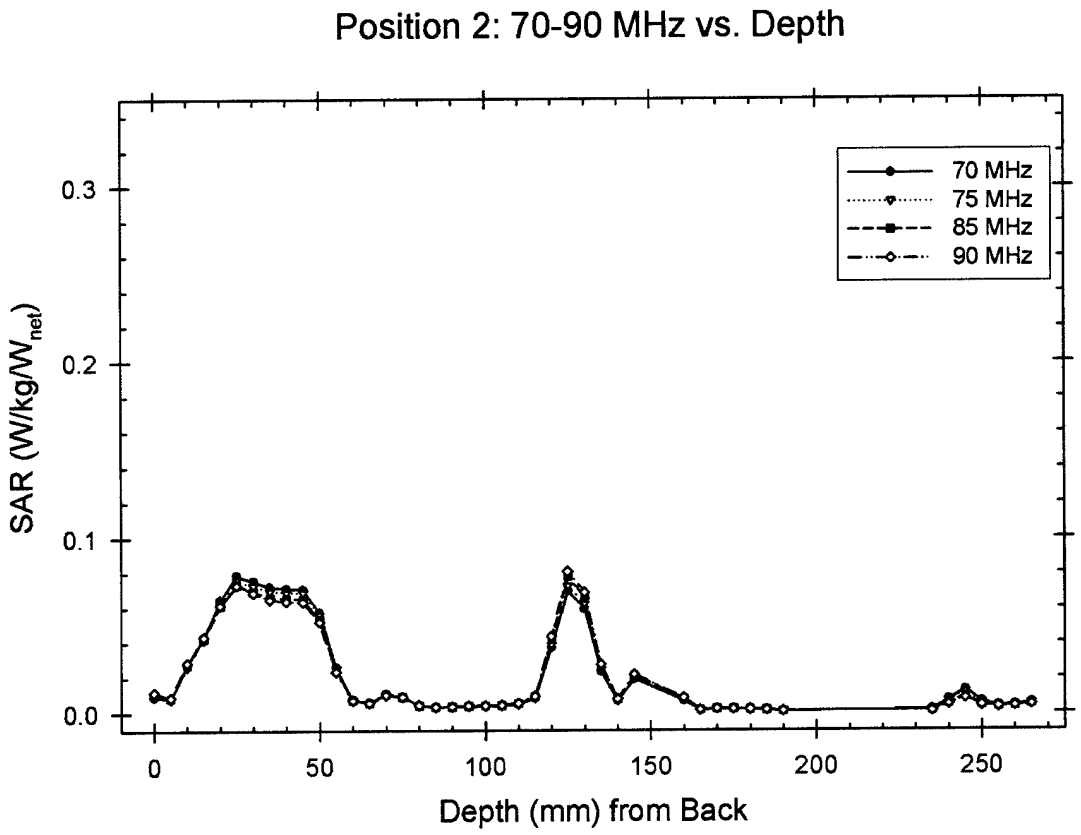

Figure 4. FDTD results (black lines) at Position 2. SAR versus depth as measured from the back surface of the anatomical model for frequencies 70, 75, 85, and 90 MHz (black symbols).

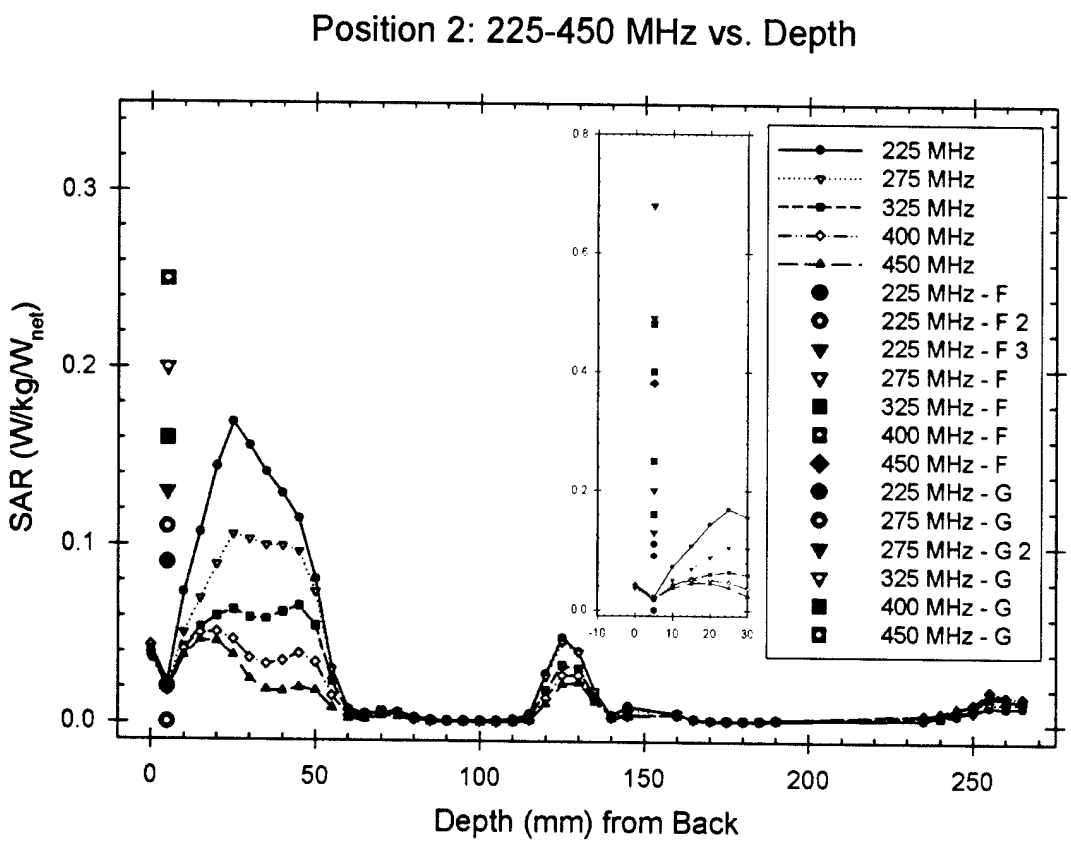

Figure 5. FDTD results (black lines) at Position 2. SAR versus depth as measured from the back surface of the anatomical model for frequencies 225, 275, 325, 400, and 450 MHz (black symbols). Empirical measurements are shown for Vest F (large blue symbols) and Vest G (large red symbols) as noted in the legend. Curves labeled with a final number indicate replicated runs. The inset figure to the left of the legend shows data that exceeds the 0.35 maximum of the main graph.

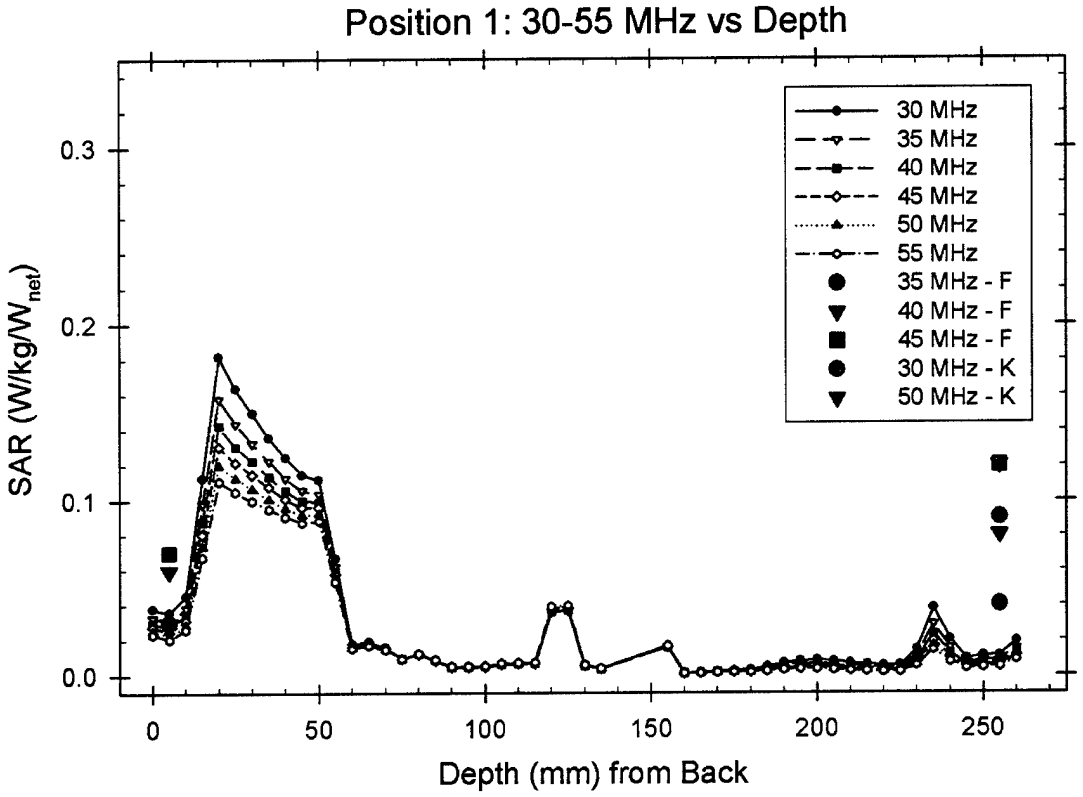

Figure 6. FDT D results (black lines) at Position 1. SAR versus depth as measured from the back surface of the anatomical model for frequencies 30, 35, 40, 45, 50 and 55 MHz (black symbols). Empirical measurements are shown for Vest F (blue symbols) and Vest K (red symbols) as noted in the legend.

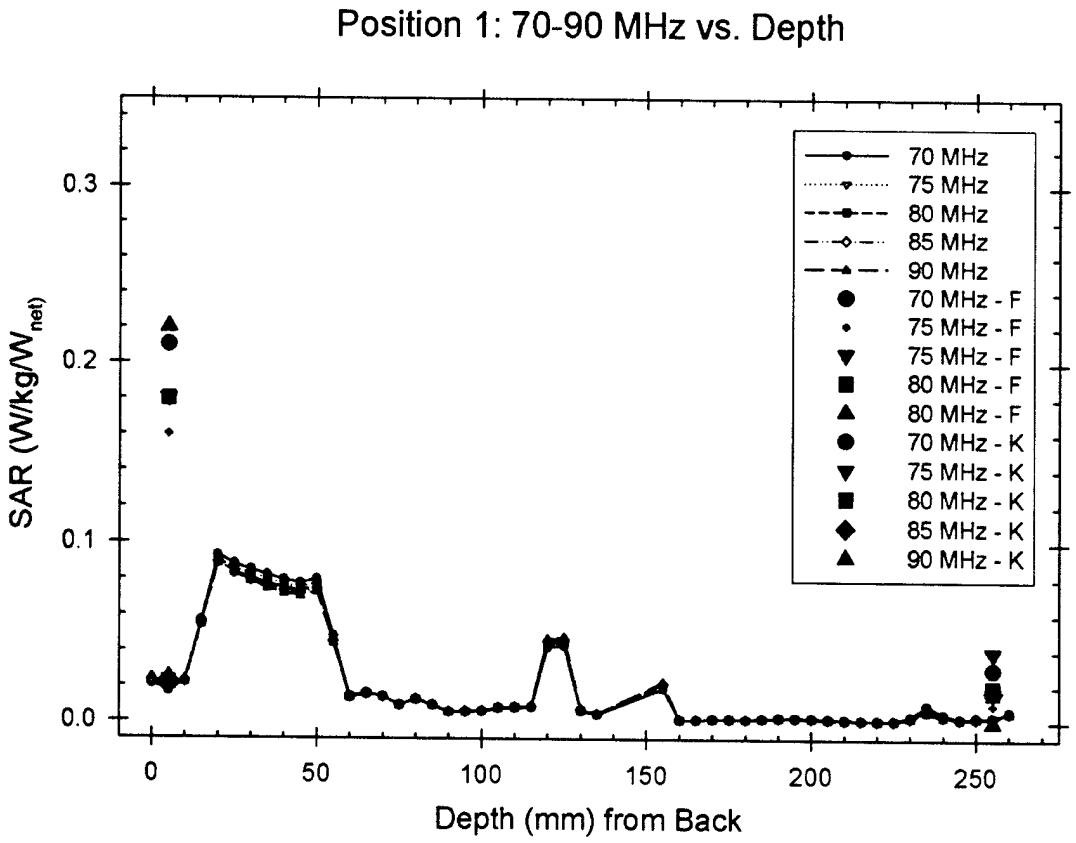

Figure 7. FDTD results (black lines) at Position 1. SAR versus depth as measured from the back surface of the anatomical model for frequencies 70, 75, 80, 85, and 90 MHz (black symbols). Empirical measurements are shown for Vest F (blue symbols) and Vest G (red symbols) as noted in the legend.

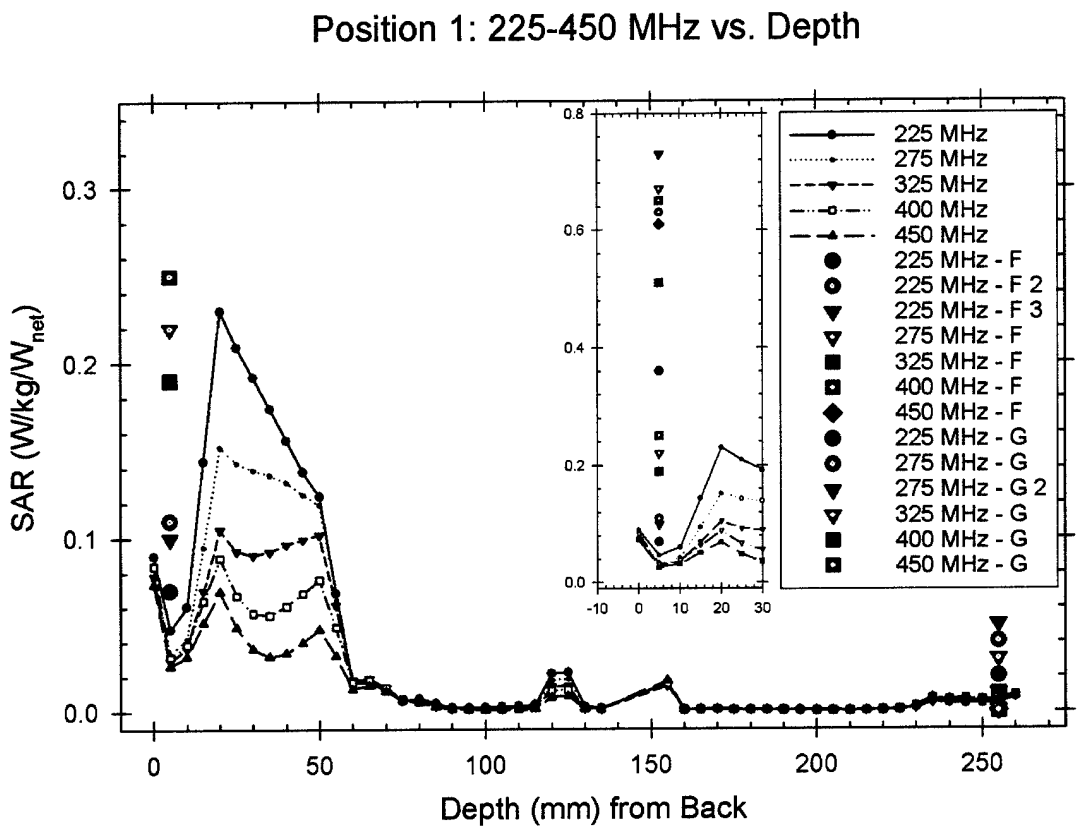

Figure 8. FDTD results (black lines) at Position 1. SAR versus depth as measured from the back surface of the anatomical model for frequencies 225, 275, 325, 400, and 450 MHz (black symbols). Empirical measurements are shown for Vest F (large blue symbols) and Vest G (large red symbols) as noted in the legend. Curves labeled with a final number indicate replicated runs. The inset figure to the left of the legend show data which exceeds the 0.35 maximum of the main graph.

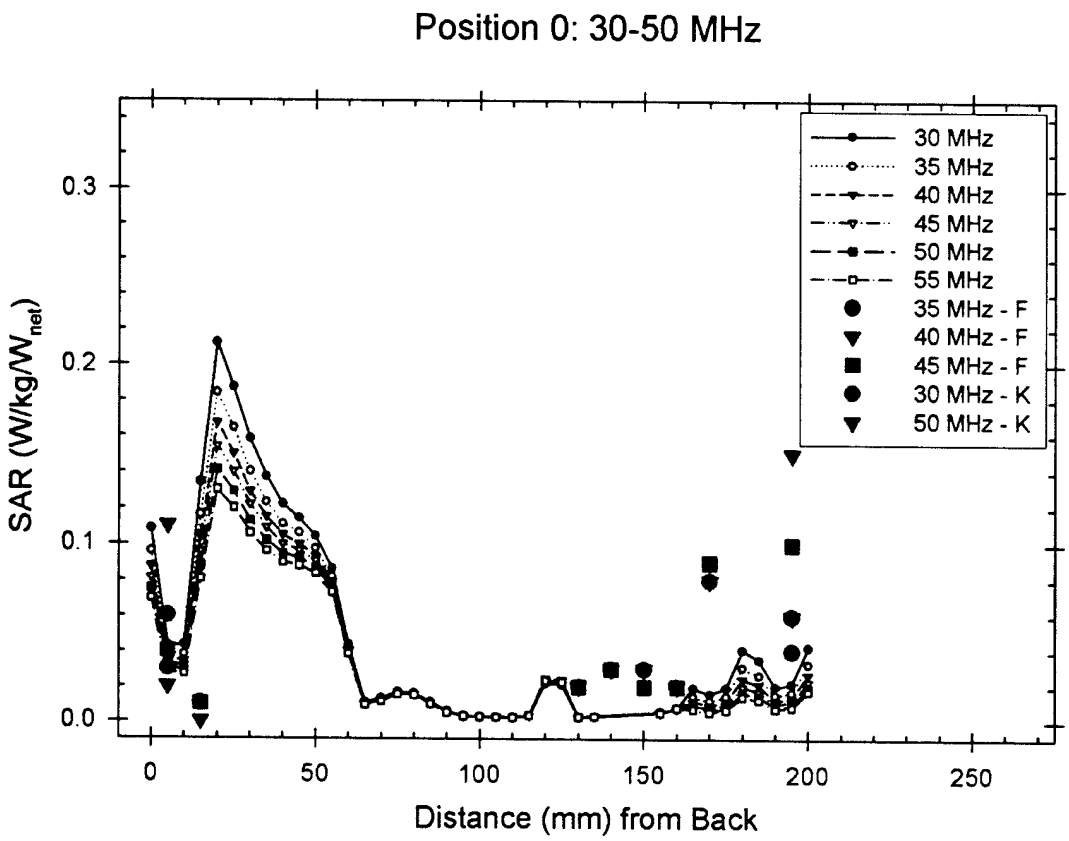

Figure 9. FDTD results (black lines) at Position 0. SAR versus depth as measured from the back surface of the anatomical model for frequencies 30, 35, 40, 45, 50, and 55 MHz (black symbols). Empirical measurements are shown for Vest F (large blue symbols) and Vest K (large red symbols) as noted in the legend.

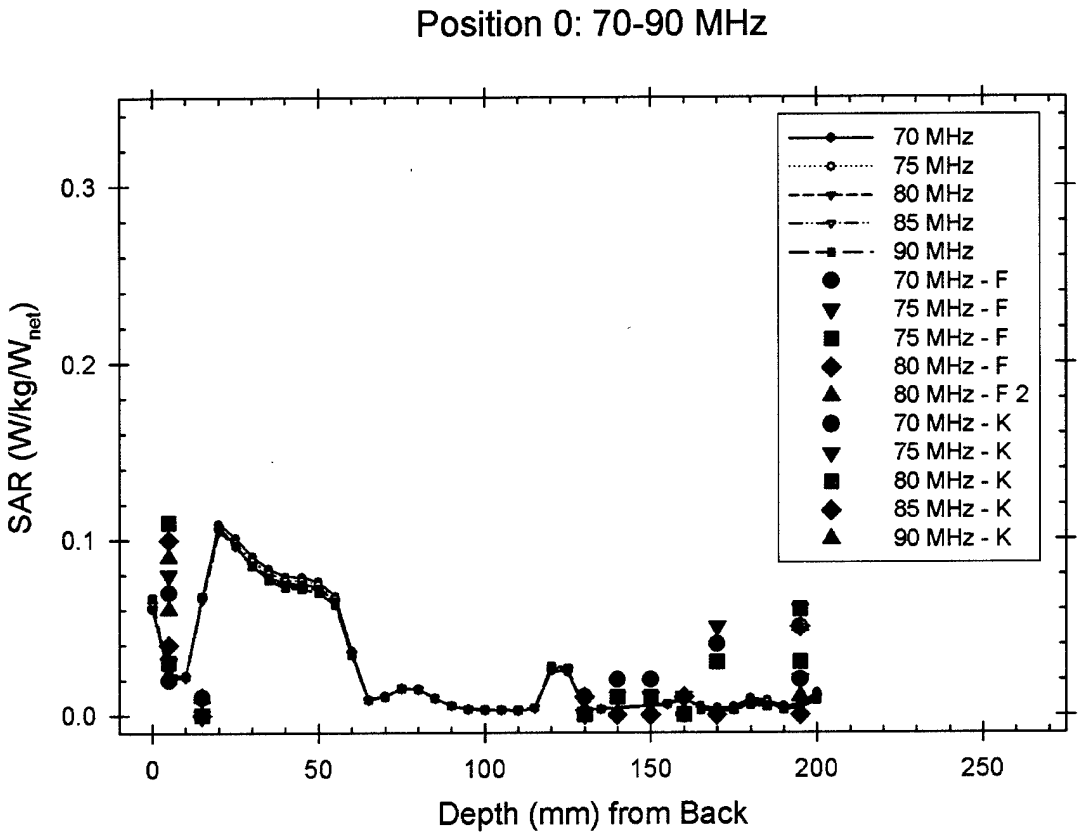

Figure 10. FDTD results (black lines) at Position 0. SAR versus depth as measured from the back surface of the anatomical model for frequencies 70, 75, 80, and 90 MHz (black symbols). Empirical measurements are shown for Vest F (large blue symbols) and Vest G (large red symbols) as noted in the legend. Curves labeled with a final number indicate replicated runs.

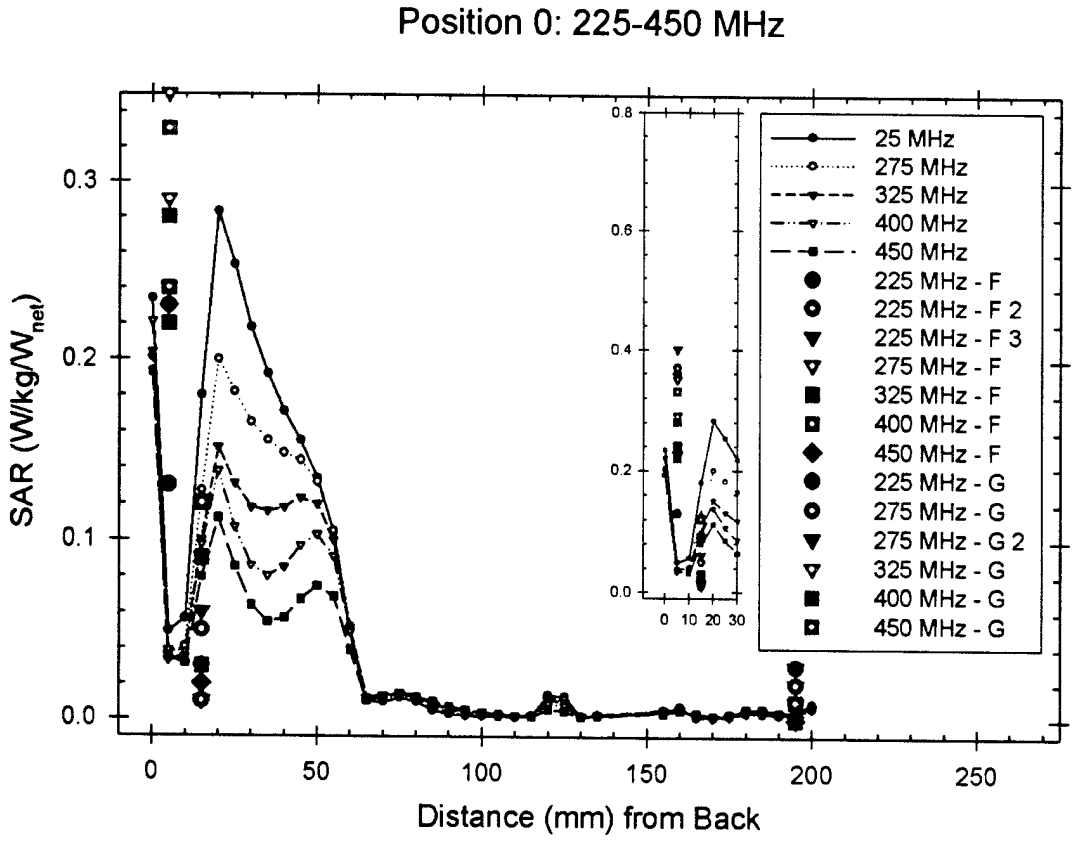

Figure 11. FDTD results (black lines) at Position 0. SAR versus depth as measured from the back surface of the anatomical model for frequencies 225, 275, 325, 400, and 450 MHz (black symbols). Empirical measurements are shown for Vest F (large blue symbols) and Vest G (large red symbols) as noted in the legend. Curves labeled with a final number indicate replicated runs. The inset figure to the left of the legend shows data that exceed the 0.35 maximum of the main graph.

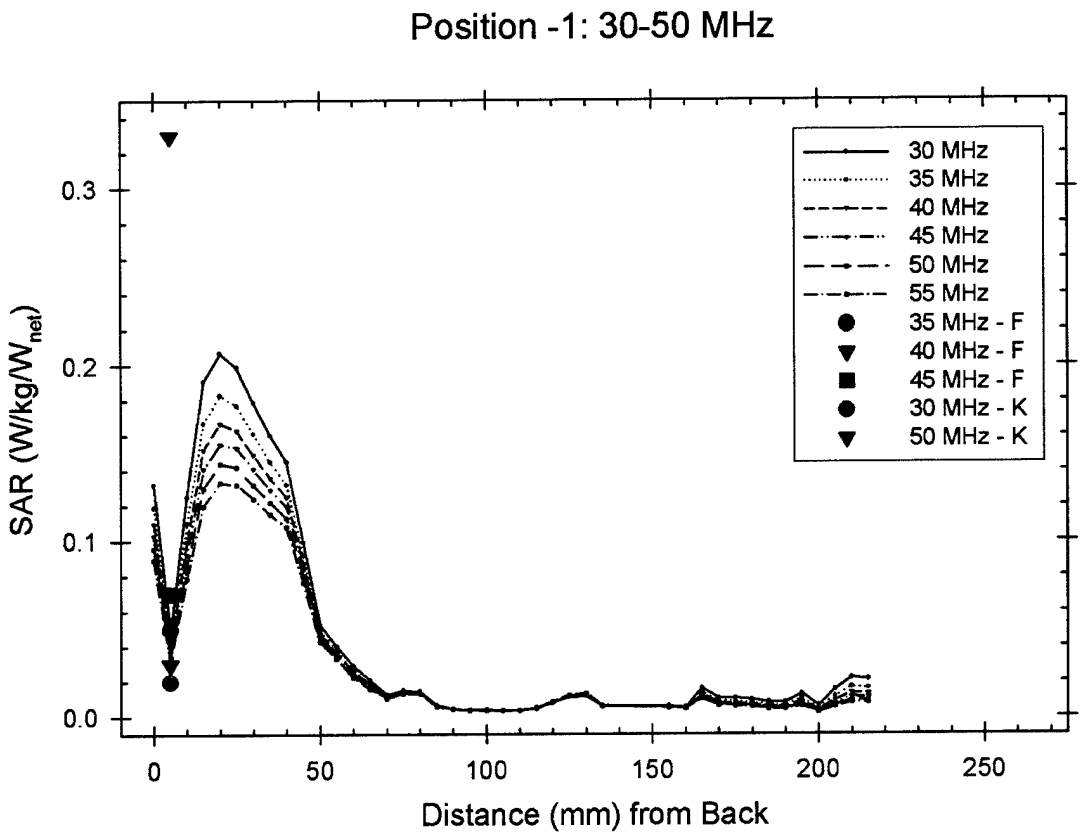

Figure 12. FDTD results (black lines) at Position 2. SAR versus depth as measured from the back surface of the anatomical model for frequencies 30, 35, 40, 45, 50, and 55 MHz (black symbols). Empirical measurements are shown for Vest F (large blue symbols) and Vest K (large red symbols) as noted in the legend.

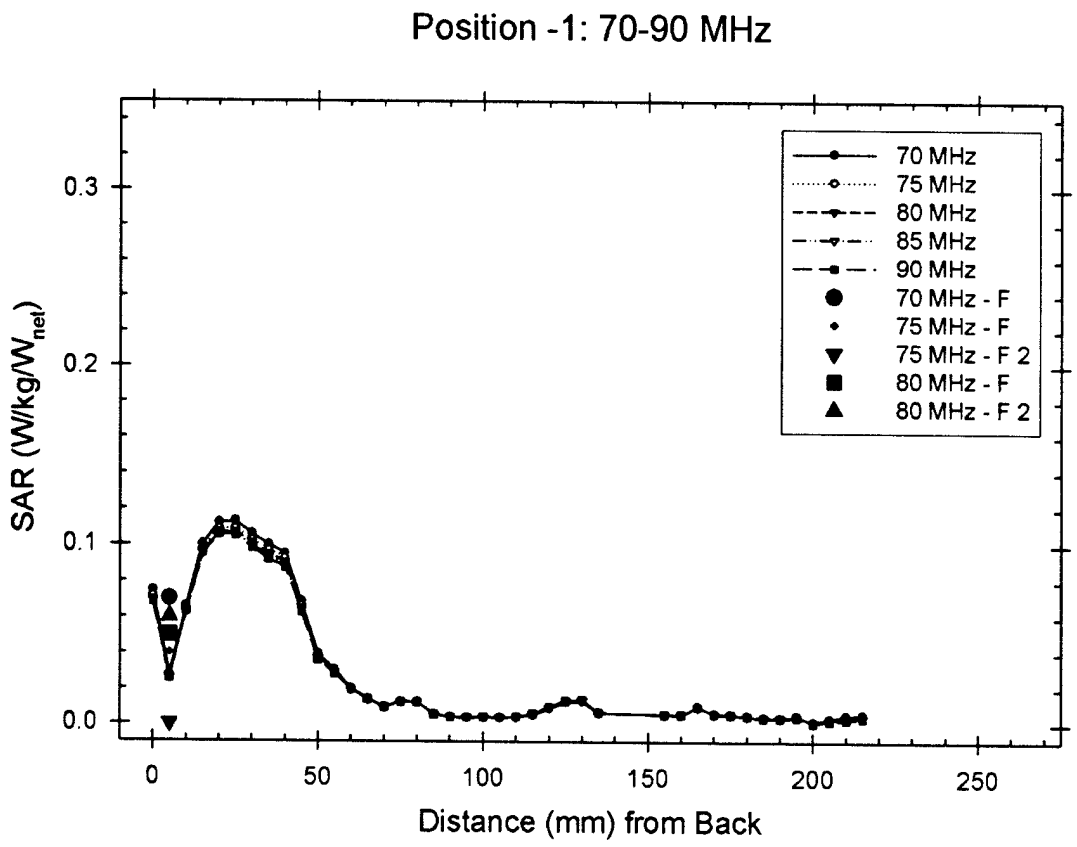

Figure 13. FDTD results (black lines) at Position -1. SAR versus depth as measured from the back surface of the anatomical model for frequencies 70, 75, 80, 85, and 90 MHz (black symbols). Empirical measurements are shown for Vest F (large blue symbols) as noted in the legend. Curves labeled with a final number indicate replicated runs.

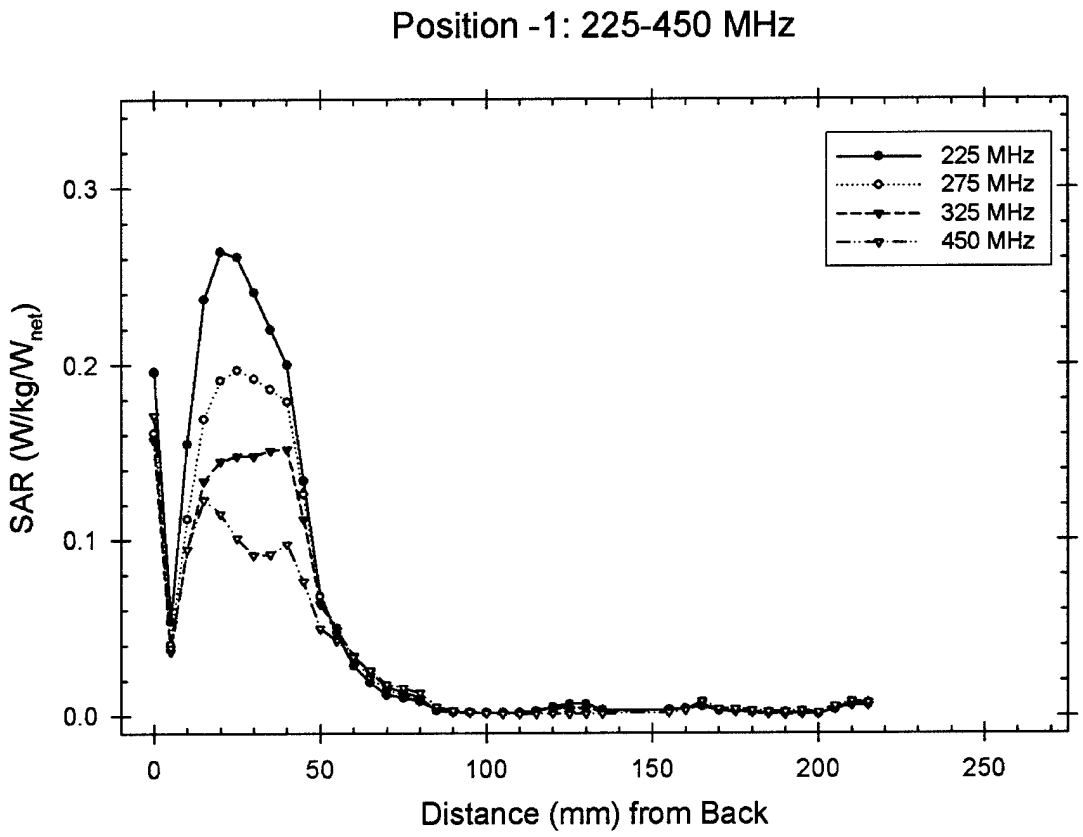

Figure 14. FDTD results (black lines) at Position -1. SAR versus depth as measured from the back surface of the anatomical model for frequencies 225, 275, 325, 400, and 450 MHz (black symbols).

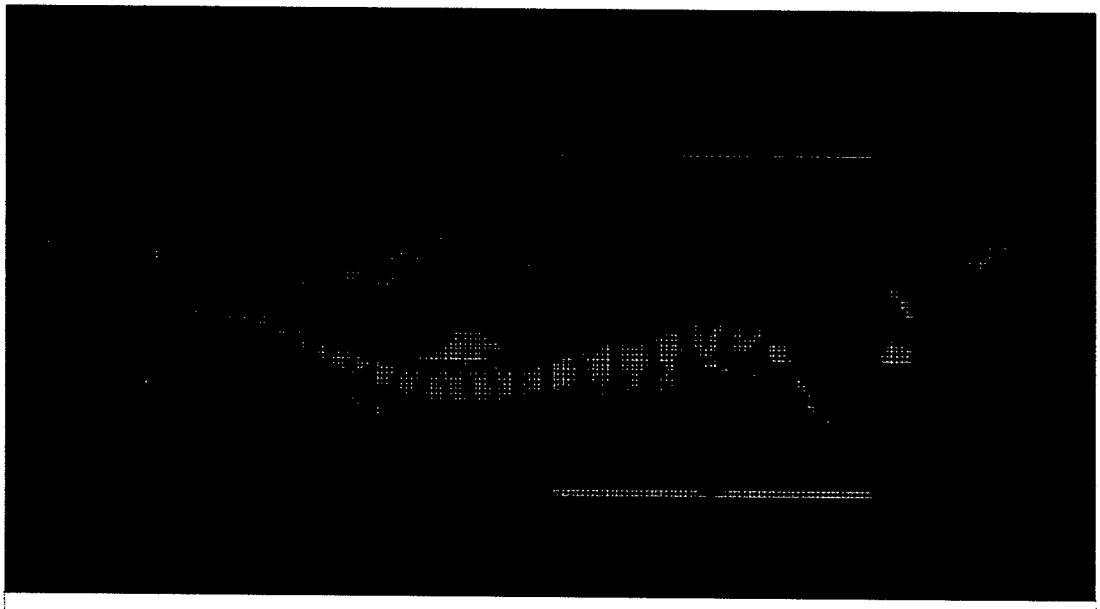

Figure 15. A mid-sagittal plane of anatomical model showing vest above and below torso. The gap in the lower band of the antenna is the feed point.

Figure 16. SAR at 30 MHz from FDTD a mid-sagittal plane.

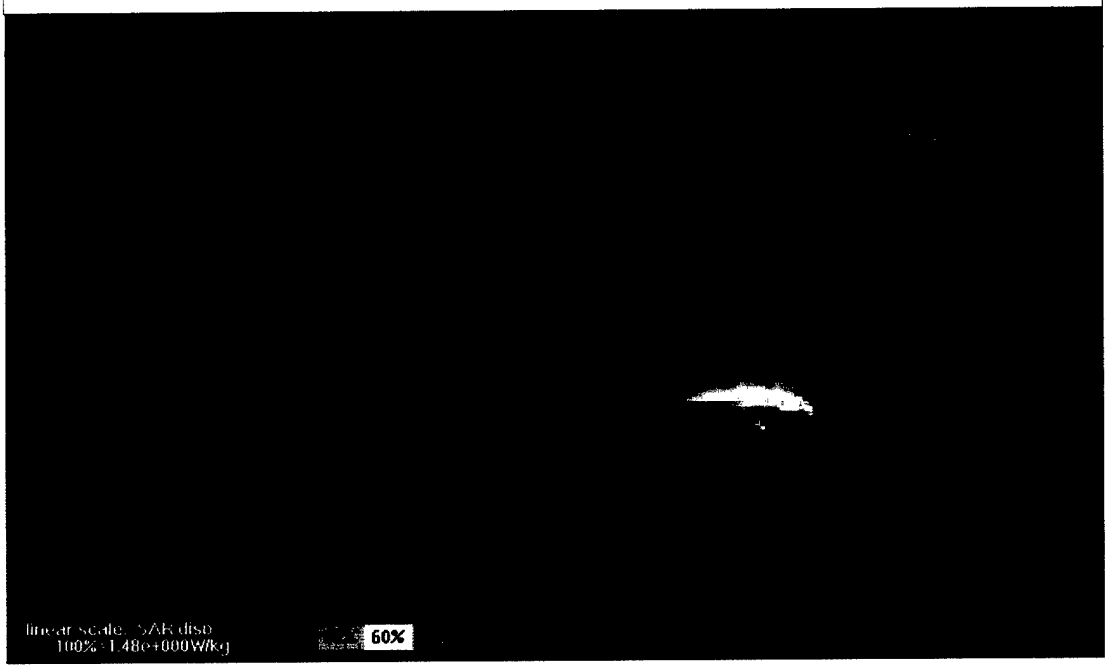

Figure 17. SAR at 35 MHz from FDTD a mid-sagittal plane.

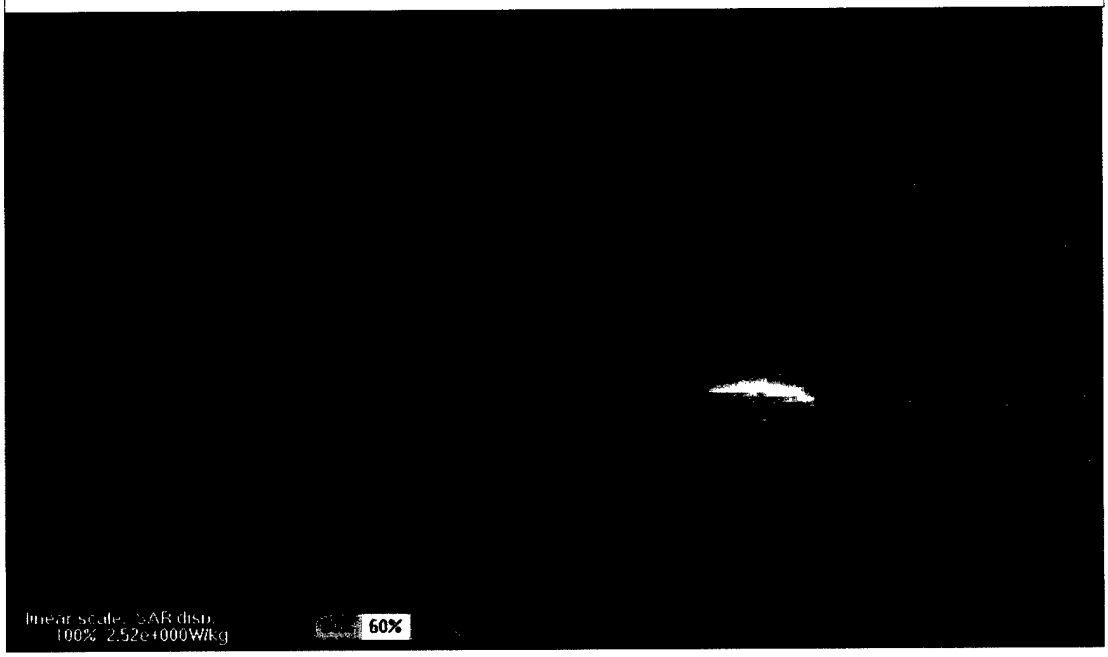

Figure 18. SAR at 40 MHz from FDTD a mid-sagittal plane.

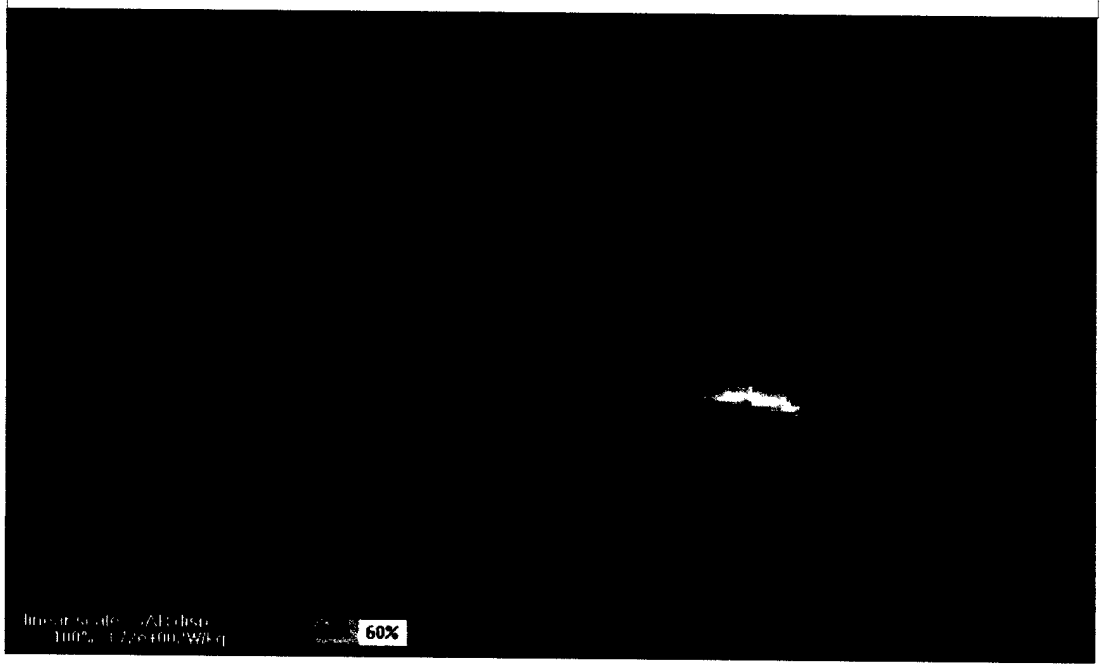

Figure 19. SAR at 45 MHz from FDTD a mid-sagittal plane.

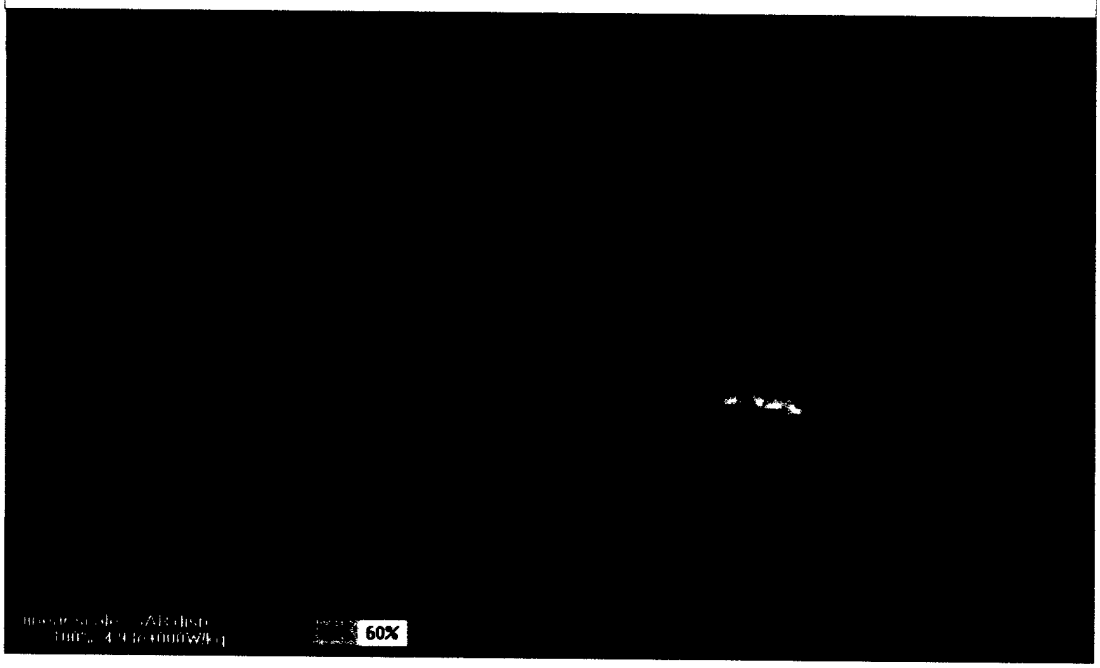

Figure 20. SAR at 50 MHz from FDTD a mid-sagittal plane.

Figure 21. SAR at 55 MHz from FDTD a mid-sagittal plane.

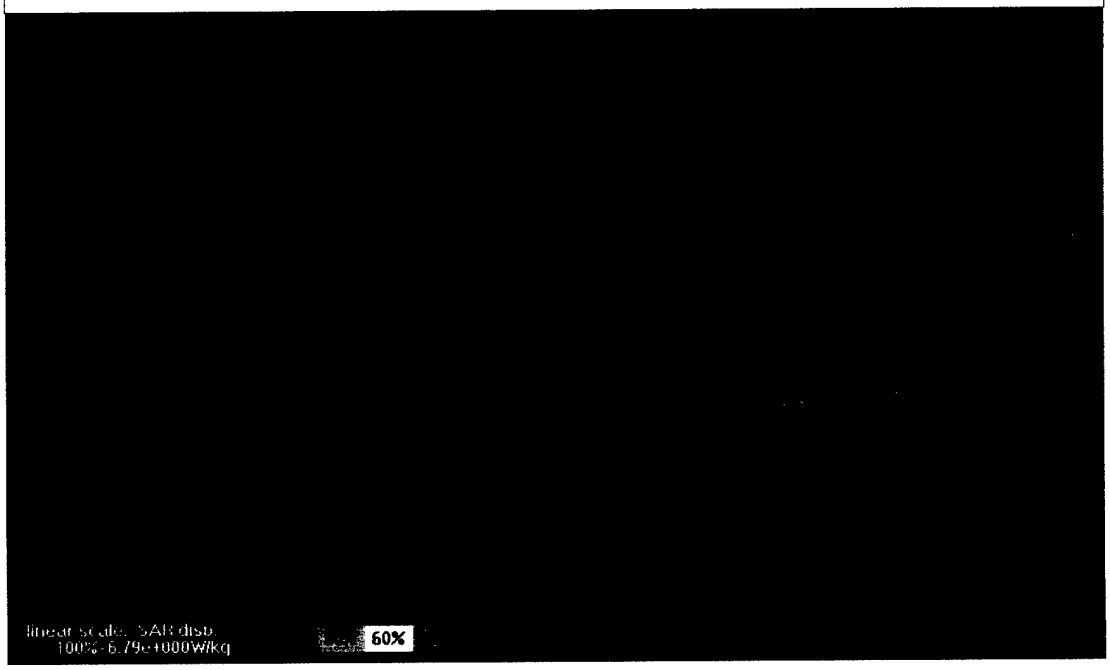

Figure 22. SAR at 70 MHz from FDTD a mid-sagittal plane.

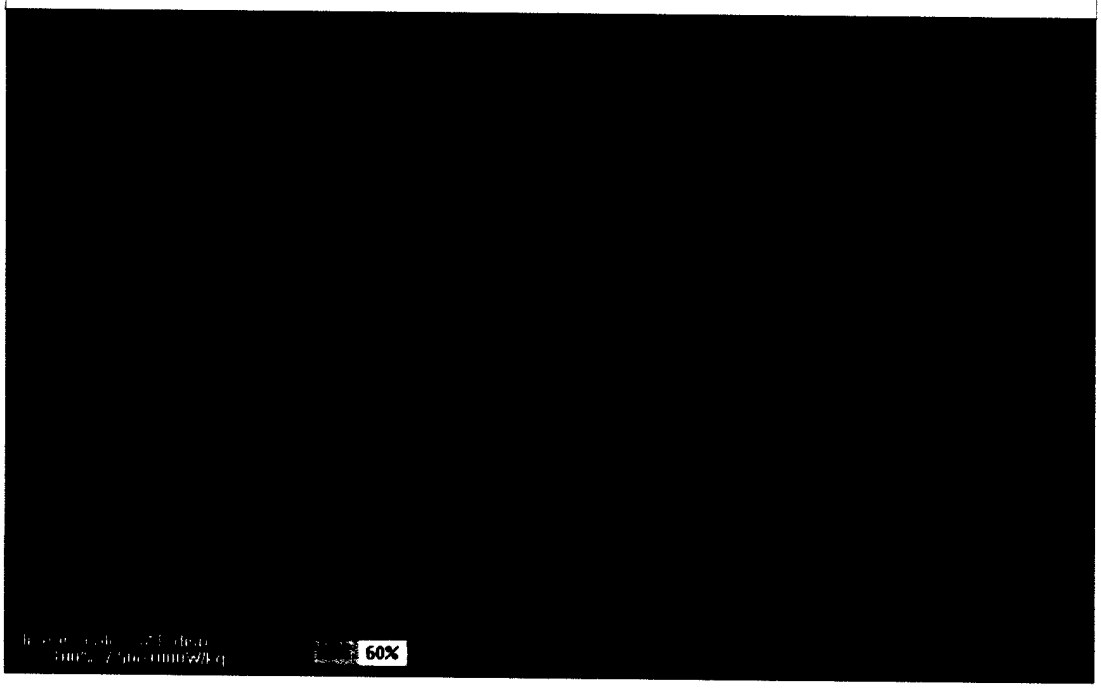

Figure 23. SAR at 75 MHz from FDTD a mid-sagittal plane.

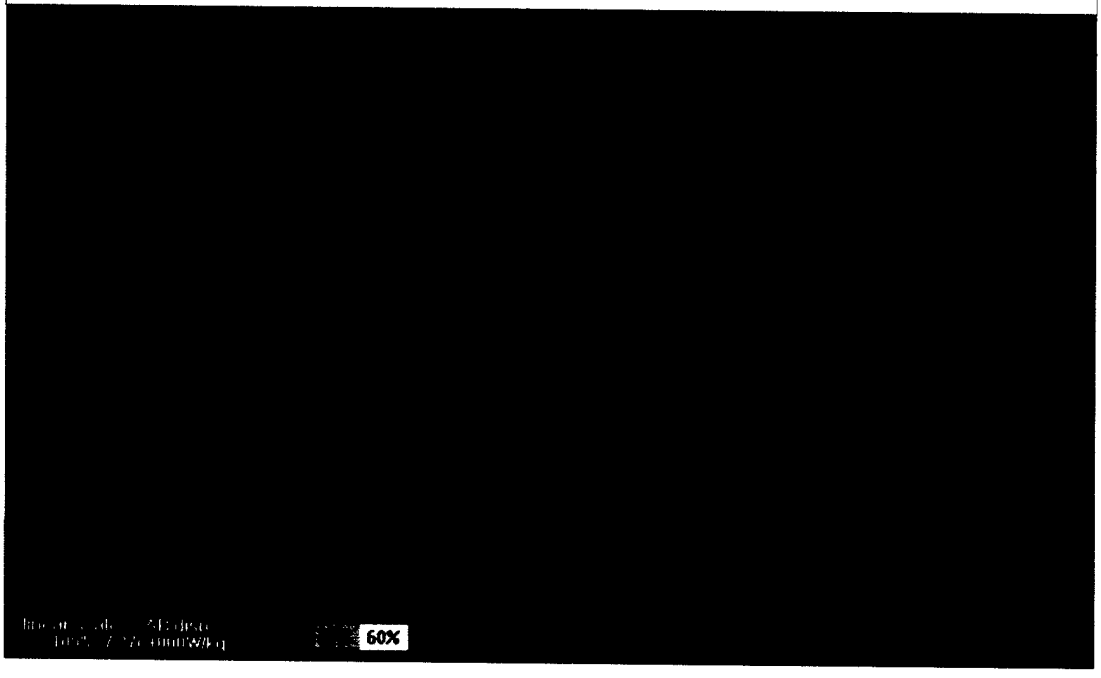

Figure 24. SAR at 80 MHz from FDTD a mid-sagittal plane.

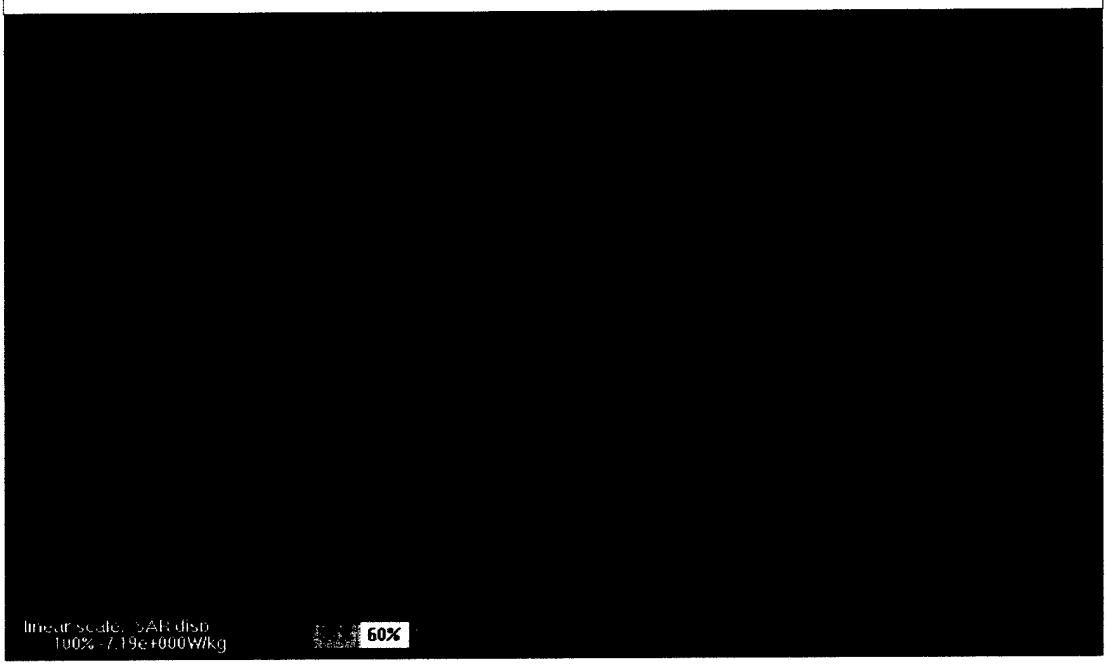

Figure 25. SAR at 85 MHz from FDTD a mid-sagittal plane.

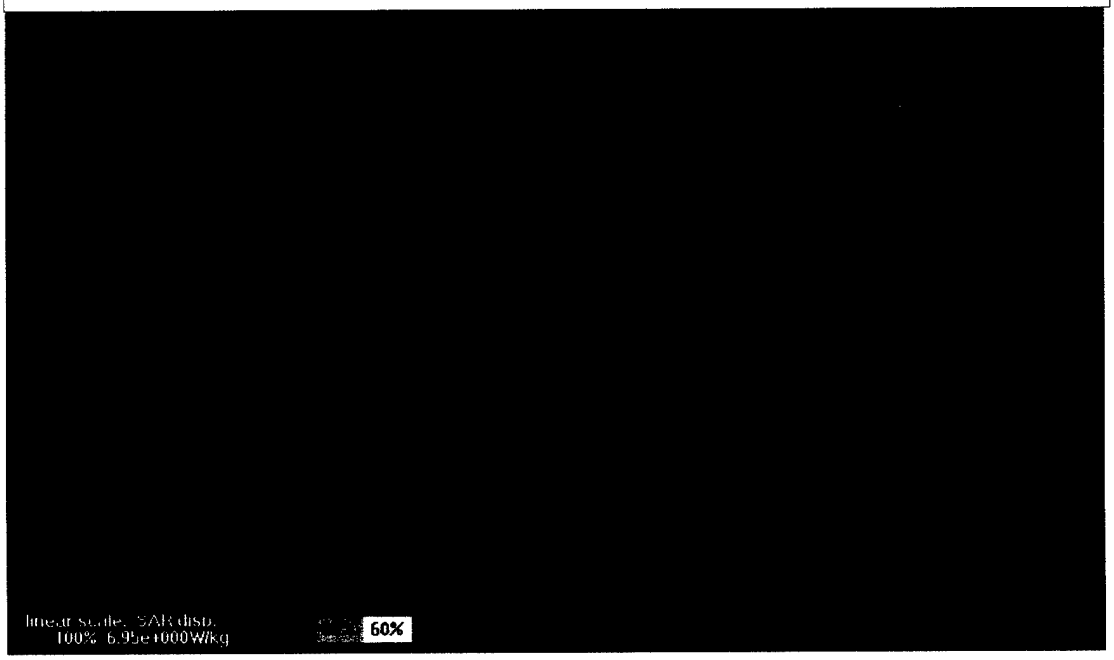

Figure 26. SAR at 90 MHz from FDTD a mid-sagittal plane.

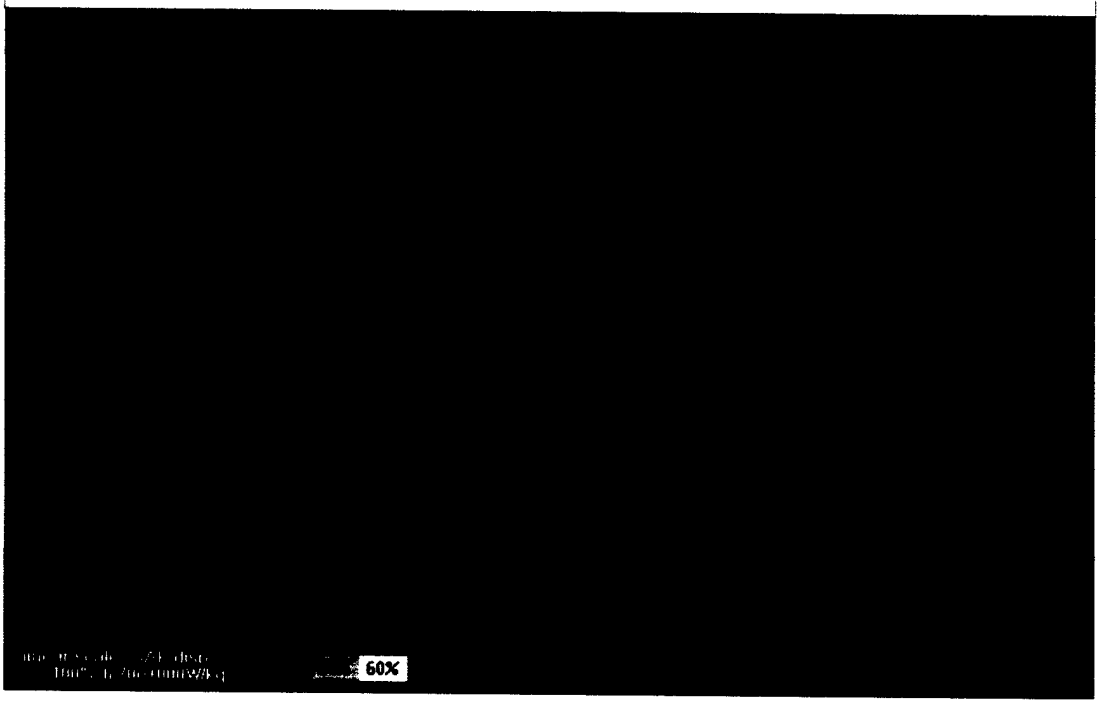

Figure 27. SAR at 225 MHz from FDTD a mid-sagittal plane.

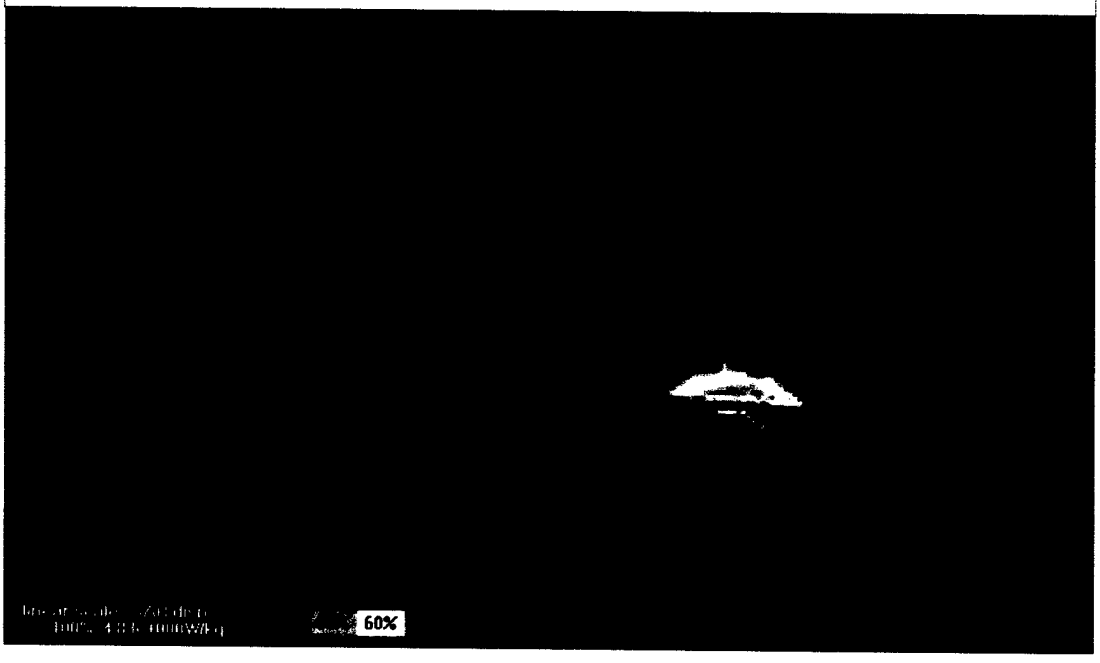

Figure 28. SAR at 275 MHz from FDTD a mid-sagittal plane.

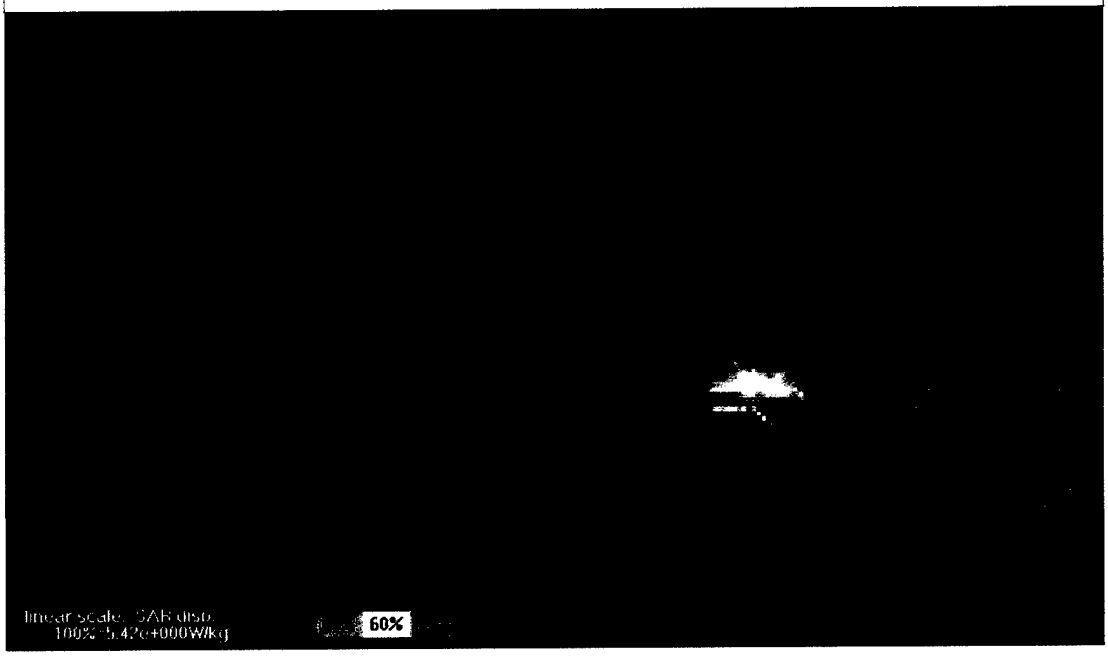

Figure 29. SAR at 325 MHz from FDTD a mid-sagittal plane.

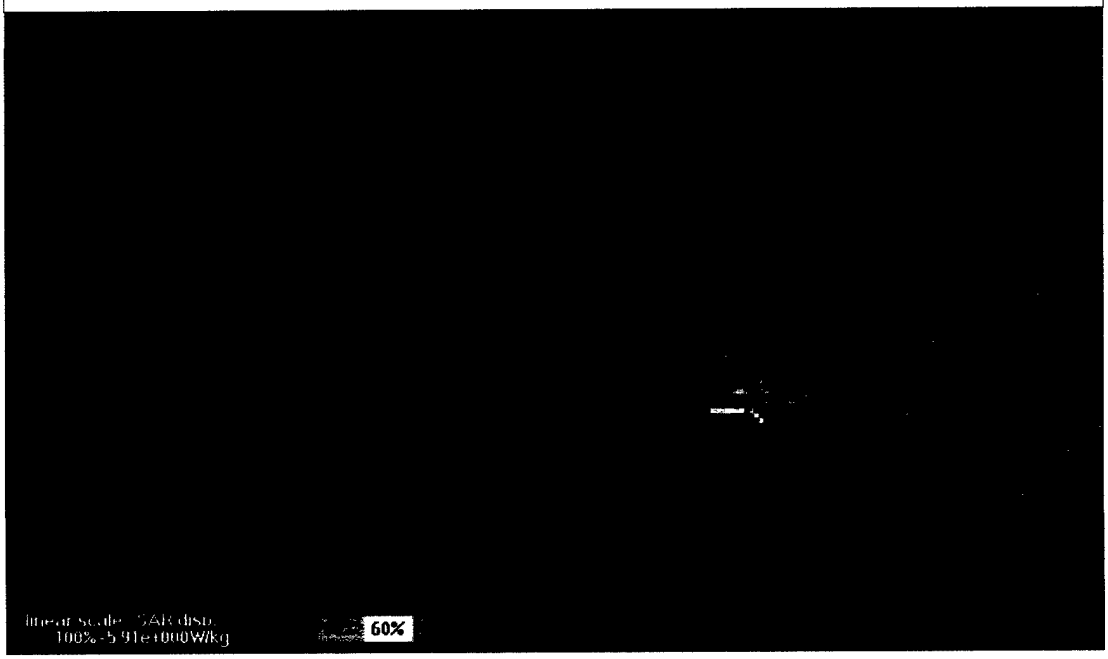

Figure 30. SAR at 400 MHz from FDTD a mid-sagittal plane.

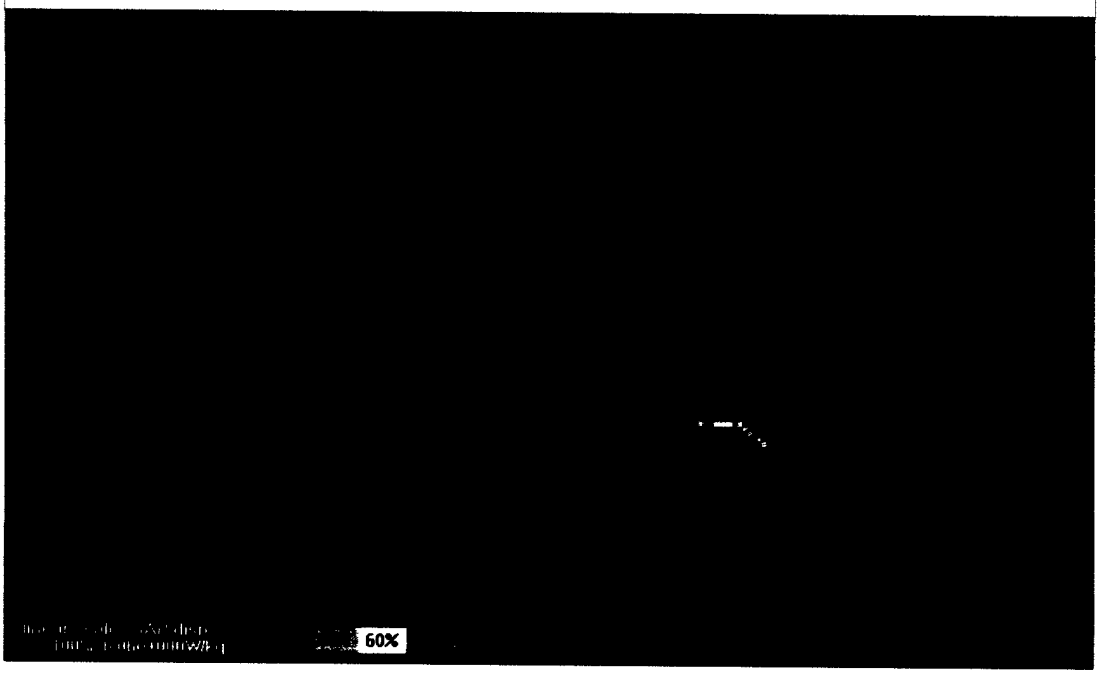

Figure 31. SAR at 450 MHz from FDTD a mid-sagittal plane.

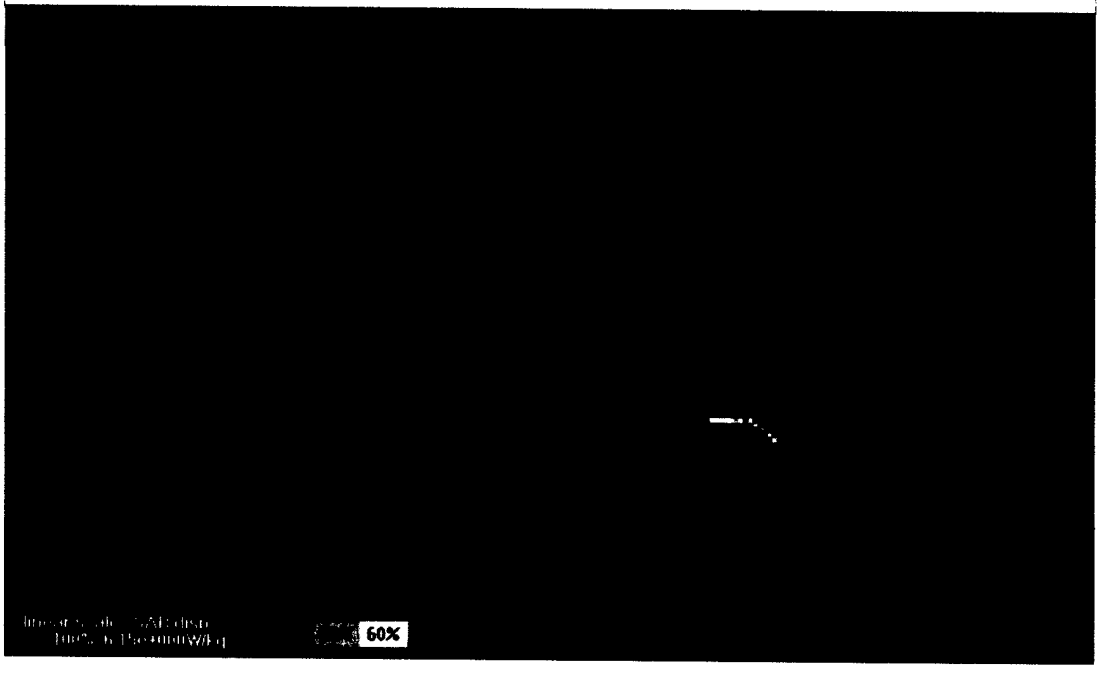

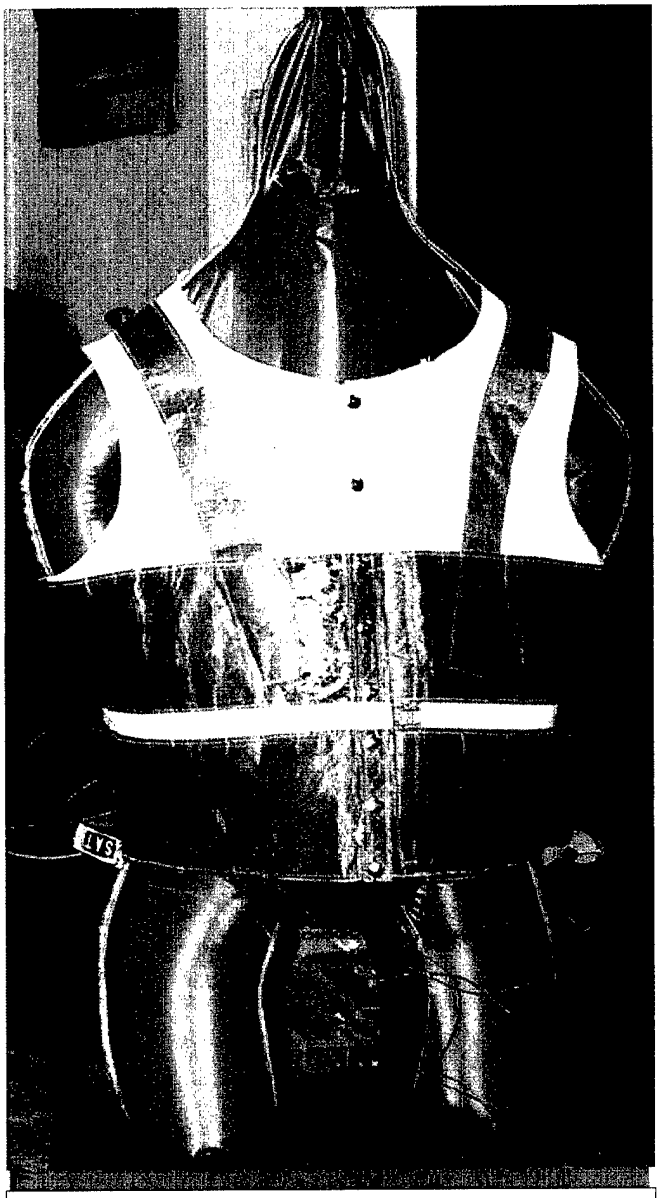

Figure 32. Front view of vest antenna and phantom.

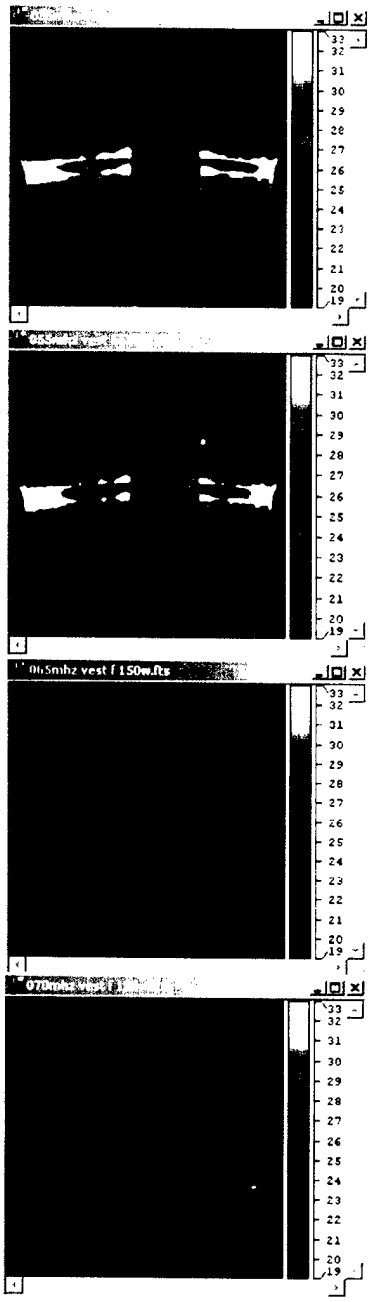

Figure 33. Infra red images of the front of Vest F at the end of 2 minute exposures at 35-70 MHz at 150 Watts net.

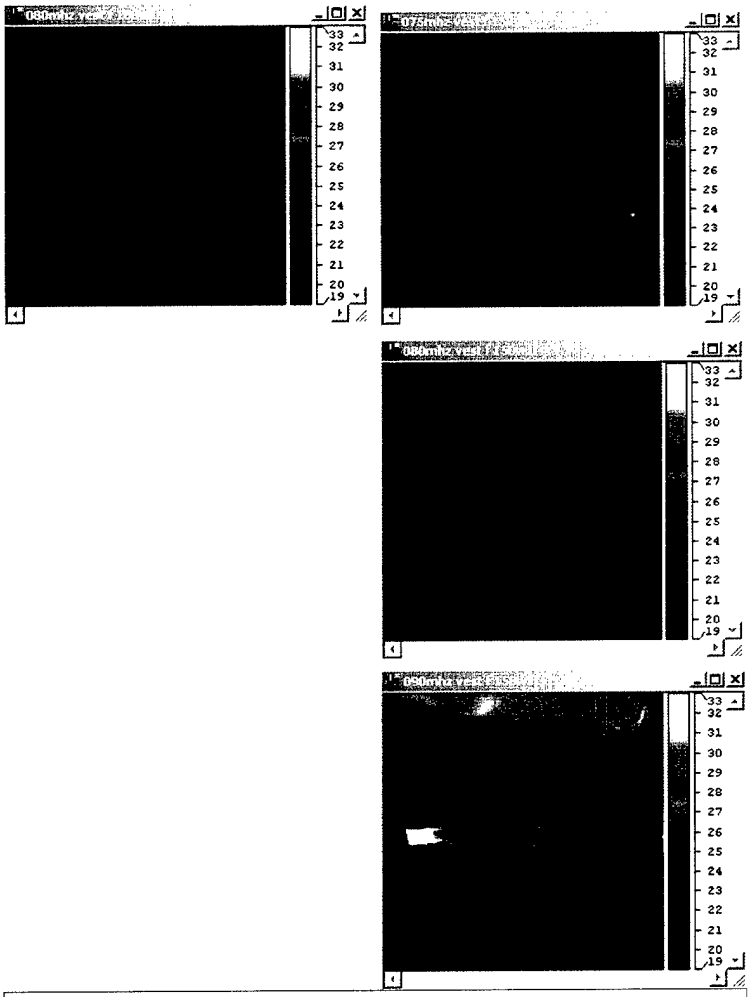

Figure 34. . Infrared front view of Vest F at 100 W net power, left column; and 200W net power, right column for 75, 80 and 90 MHz.

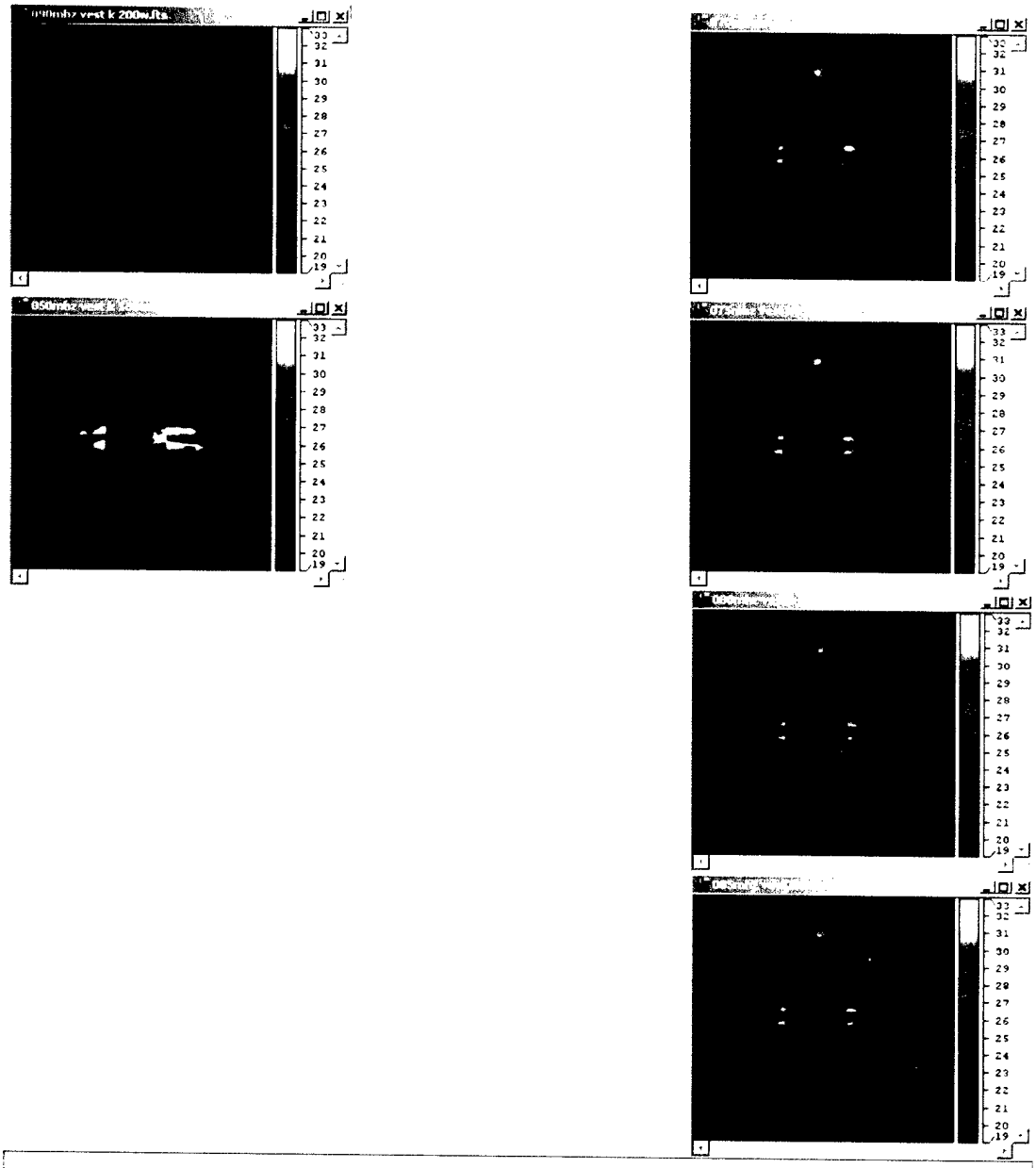

Figure 35. Infrared images of front view of Vest K for 50 to 90 MHz at 100 W, left column, and 200 W, right column, net power

LIST OF TABLES

Table 1. Vest F (Part 1 of 3): List of runs, probe locations, probe numbers, measured SARs per Watt of net power, and SAR normalized to a 5W net power.

File	Side	Position	Depth	Probe#	Frequency (MHz)	Run	Power (W)	SAR/W	SAR/ 5W
1	B	-1	0.5	5	35	1	94	0.046	0.230
2	B	-1	0.5	5	40	1	200	0.032	0.161
3	B	-1	0.5	5	45	1	200	0.074	0.368
7	B	-1	0.5	5	70	1	150	0.070	0.348
6	B	-1	0.5	5	75	1	100	0.040	0.201
8	B	-1	0.5	5	75	2	150	0.000	0.001
4	B	-1	0.5	5	80	1	100	0.046	0.228
5	B	-1	0.5	5	80	2	150	0.063	0.314
1	B	0	0.5	2	35	1	94	0.027	0.137
2	B	0	0.5	2	40	1	200	0.019	0.097
3	B	0	0.5	2	45	1	200	0.036	0.181
7	B	0	0.5	2	70	1	150	0.017	0.086
6	B	0	0.5	2	75	1	100	0.026	0.132
8	B	0	0.5	2	75	2	150	0.030	0.151
4	B	0	0.5	2	80	1	100	0.040	0.198
5	B	0	0.5	2	80	2	150	0.059	0.296
10	B	0	0.5	2	225	1	100	0.132	0.658
11	B	0	0.5	2	225	1	150	0.228	1.142
12	B	0	0.5	2	225	2	150	0.242	1.212
22	B	0	0.5	2	275	1	150	0.351	1.757
21	B	0	0.5	2	325	1	150	0.222	1.112
20	B	0	0.5	2	400	1	150	0.238	1.191
19	B	0	0.5	2	450	1	150	0.228	1.141
1	B	0	1.5	3	35	1	94	0.010	0.052
2	B	0	1.5	3	40	1	200	0.005	0.025
3	B	0	1.5	3	45	1	200	0.013	0.063
7	B	0	1.5	3	70	1	150	0.007	0.035
6	B	0	1.5	3	75	1	100	0.000	0.001
8	B	0	1.5	3	75	2	150	0.003	0.016
4	B	0	1.5	3	80	1	100	0.000	0.001
5	B	0	1.5	3	80	2	150	0.011	0.054
10	B	0	1.5	3	225	1	100	0.005	0.026
11	B	0	1.5	3	225	1	150	0.006	0.029
12	B	0	1.5	3	225	2	150	0.013	0.066
22	B	0	1.5	3	275	1	150	0.013	0.063
21	B	0	1.5	3	325	1	150	0.030	0.151
20	B	0	1.5	3	400	1	150	0.028	0.142
19	B	0	1.5	3	450	1	150	0.022	0.112
1	B	1	0.5	6	35	1	94	0.034	0.170
2	B	1	0.5	6	40	1	200	0.029	0.146
3	B	1	0.5	6	45	1	200	0.069	0.346

Table 2. Vest F (Part 2 of 3): List of runs, probe locations, probe numbers, measured SARs per Watt of net power, and SAR normalized to a 5W net power.

File	Side	Position	Depth	Probe#	Frequency	Run	Power (W)	SAR/W	SAR/ 5W
7	B	1	0.5	6	70	1	150	0.206	1.031
6	B	1	0.5	6	75	1	100	0.157	0.783
8	B	1	0.5	6	75	2	150	0.184	0.922
4	B	1	0.5	6	80	1	100	0.178	0.889
5	B	1	0.5	6	80	2	150	0.225	1.125
10	B	1	0.5	6	225	1	100	0.364	1.820
11	B	1	0.5	6	225	1	150	0.633	3.166
12	B	1	0.5	6	225	2	150	0.734	3.670
22	B	1	0.5	6	275	1	150	0.670	3.350
21	B	1	0.5	6	325	1	150	0.513	2.566
20	B	1	0.5	6	400	1	150	0.648	3.241
19	B	1	0.5	6	450	1	150	0.610	3.049
10	B	2	0.5	5	225	1	100	0.020	0.099
11	B	2	0.5	5	225	1	150	0.003	0.016
12	B	2	0.5	5	225	2	150	0.684	3.422
22	B	2	0.5	5	275	1	150	0.489	2.443
21	B	2	0.5	5	325	1	150	0.403	2.016
20	B	2	0.5	5	400	1	150	0.483	2.417
19	B	2	0.5	5	450	1	150	0.377	1.887
1	F	0	0.5	1	35	1	94	0.063	0.317
2	F	0	0.5	1	40	1	200	0.059	0.293
3	F	0	0.5	1	45	1	200	0.098	0.491
7	F	0	0.5	1	70	1	150	0.025	0.124
6	F	0	0.5	1	75	1	100	0.017	0.086
8	F	0	0.5	1	75	2	150	0.033	0.165
4	F	0	0.5	1	80	1	100	0.000	0.001
5	F	0	0.5	1	80	2	150	0.009	0.046
10	F	0	0.5	1	225	1	100	0.009	0.046
11	F	0	0.5	1	225	1	150	0.029	0.147
12	F	0	0.5	1	225	2	150	0.006	0.029
22	F	0	0.5	1	275	1	150	0.000	0.001
21	F	0	0.5	1	325	1	150	0.004	0.019
20	F	0	0.5	1	400	1	150	0.000	0.001
19	F	0	0.5	1	450	1	150	0.005	0.024
29	F	0	3	2	35	1	150	0.083	0.416
28	F	0	3	2	40	1	150	0.085	0.423
27	F	0	3	2	55	1	150	0.091	0.457
26	F	0	3	2	70	2	150	0.036	0.182
25	F	0	3	2	75	3	150	0.052	0.259
24	F	0	3	2	80	3	150	0.032	0.158
23	F	0	3	2	90	1	150	0.004	0.018
29	F	0	4	3	35	1	150	0.017	0.086
28	F	0	4	3	40	1	150	0.017	0.086

Table 3. Vest F (Part 3 of 3): List of runs, probe locations, probe numbers, measured SARs per Watt of net power, and SAR normalized to a 5W net power.

File	Side	Position	Depth	Probe#	Frequency (MHz)	Run	Power (W)	SAR/W	SAR/ 5W
27	F	0	4	3	55	1	150	0.021	0.107
26	F	0	4	3	70	2	150	0.002	0.009
25	F	0	4	3	75	3	150	0.009	0.043
24	F	0	4	3	80	3	150	0.000	0.001
23	F	0	4	3	90	1	150	0.005	0.026
29	F	0	5	4	35	1	150	0.031	0.153
28	F	0	5	4	40	1	150	0.031	0.153
27	F	0	5	4	55	1	150	0.021	0.107
26	F	0	5	4	70	2	150	0.015	0.076
25	F	0	5	4	75	3	150	0.009	0.043
24	F	0	5	4	80	3	150	0.014	0.070
23	F	0	5	4	90	1	150	0.000	0.001
29	F	0	6	5	35	1	150	0.031	0.154
28	F	0	6	5	40	1	150	0.034	0.172
27	F	0	6	5	55	1	150	0.032	0.162
26	F	0	6	5	70	2	150	0.015	0.077
25	F	0	6	5	75	3	150	0.006	0.031
24	F	0	6	5	80	3	150	0.014	0.068
23	F	0	6	5	90	1	150	0.000	0.001
29	F	0	7	6	35	1	150	0.023	0.113
28	F	0	7	6	40	1	150	0.017	0.086
27	F	0	7	6	55	1	150	0.020	0.099
26	F	0	7	6	70	2	150	0.006	0.031
25	F	0	7	6	75	3	150	0.004	0.019
24	F	0	7	6	80	3	150	0.001	0.004
23	F	0	7	6	90	1	150	0.005	0.027
1	F	1	0.5	4	35	1	94	0.088	0.439
2	F	1	0.5	4	40	1	200	0.081	0.405
3	F	1	0.5	4	45	1	200	0.119	0.593
7	F	1	0.5	4	70	1	150	0.035	0.175
6	F	1	0.5	4	75	1	100	0.008	0.040
8	F	1	0.5	4	75	2	150	0.036	0.181
4	F	1	0.5	4	80	1	100	0.025	0.125
5	F	1	0.5	4	80	2	150	0.000	0.001
10	F	1	0.5	4	225	1	100	0.003	0.014
11	F	1	0.5	4	225	1	150	0.004	0.019
12	F	1	0.5	4	225	2	150	0.002	0.012
22	F	1	0.5	4	275	1	150	0.014	0.070
21	F	1	0.5	4	325	1	150	0.010	0.048
20	F	1	0.5	4	400	1	150	0.006	0.029
19	F	1	0.5	4	450	1	150	0.002	0.008

Table 4. Vest G: List of runs, probe locations, probe numbers, measured SARs per Watt of net power, and SAR normalized to a 5W net power.

File	Side	Position	Depth	Probe#	Frequency (MHz)	Run	Power (W)	SAR/W	SAR/ 5W
13	B	0	0.5	2	225	3	150	0.360	1.799
14	B	0	0.5	2	275	1	100	0.371	1.854
15	B	0	0.5	2	275	1	150	0.397	1.983
16	B	0	0.5	2	325	1	150	0.291	1.456
17	B	0	0.5	2	400	1	150	0.277	1.387
18	B	0	0.5	2	450	1	150	0.325	1.626
13	B	0	1.5	3	225	3	150	0.032	0.161
14	B	0	1.5	3	275	1	100	0.053	0.263
15	B	0	1.5	3	275	1	150	0.057	0.284
16	B	0	1.5	3	325	1	150	0.094	0.470
17	B	0	1.5	3	400	1	150	0.091	0.457
18	B	0	1.5	3	450	1	150	0.121	0.603
13	B	1	0.5	6	225	3	150	0.069	0.344
14	B	1	0.5	6	275	1	100	0.105	0.526
15	B	1	0.5	6	275	1	150	0.097	0.486
16	B	1	0.5	6	325	1	150	0.216	1.081
17	B	1	0.5	6	400	1	150	0.190	0.951
18	B	1	0.5	6	450	1	150	0.251	1.256
13	B	2	0.5	5	225	3	150	0.089	0.446
14	B	2	0.5	5	275	1	100	0.107	0.536
15	B	2	0.5	5	275	1	150	0.130	0.649
16	B	2	0.5	5	325	1	150	0.200	0.998
17	B	2	0.5	5	400	1	150	0.158	0.788
18	B	2	0.5	5	450	1	150	0.251	1.257
13	F	0	0.5	1	225	3	150	0.016	0.082
14	F	0	0.5	1	275	1	100	0.028	0.140
15	F	0	0.5	1	275	1	150	0.035	0.174
16	F	0	0.5	1	325	1	150	0.017	0.084
17	F	0	0.5	1	400	1	150	0.005	0.027
18	F	0	0.5	1	450	1	150	0.011	0.054
13	F	1	0.5	4	225	3	150	0.018	0.091
14	F	1	0.5	4	275	1	100	0.039	0.196
15	F	1	0.5	4	275	1	150	0.046	0.228
16	F	1	0.5	4	325	1	150	0.031	0.157
17	F	1	0.5	4	400	1	150	0.013	0.067
18	F	1	0.5	4	450	1	150	0.005	0.024

Table 5. Vest K: List of runs, probe locations, probe numbers, measured SARs per Watt of net power, and SAR normalized to a 5W net power.

File	Side	Position	Depth	Probe#	Frequency (MHz)	Run	Power (W)	SAR/W	SAR/ 5W
30	B	-1	0.5	3	30	1	150	0.018	0.088
31	B	-1	0.5	3	50	1	150	0.330	1.650
36	B	-1	0.5	3	70	1	200	0.024	0.121
32	B	-1	0.5	3	75	1	200	0.020	0.100
33	B	-1	0.5	3	80	1	200	0.026	0.129
34	B	-1	0.5	3	85	1	200	0.030	0.151
35	B	-1	0.5	3	90	1	200	0.029	0.144
30	B	0	0.5	5	30	1	150	0.056	0.282
31	B	0	0.5	5	50	1	150	0.113	0.566
36	B	0	0.5	5	70	1	200	0.070	0.351
32	B	0	0.5	5	75	1	200	0.084	0.418
33	B	0	0.5	5	80	1	200	0.105	0.527
34	B	0	0.5	5	85	1	200	0.101	0.506
35	B	0	0.5	5	90	1	200	0.092	0.462
30	B	1	0.5	6	30	1	150	0.026	0.130
31	B	1	0.5	6	50	1	150	0.058	0.289
36	B	1	0.5	6	70	1	200	0.048	0.238
32	B	1	0.5	6	75	1	200	0.062	0.308
33	B	1	0.5	6	80	1	200	0.066	0.328
34	B	1	0.5	6	85	1	200	0.072	0.361
35	B	1	0.5	6	90	1	200	0.072	0.358
30	F	0	0.5	1	30	1	150	0.045	0.223
31	F	0	0.5	1	50	1	150	0.155	0.774
36	F	0	0.5	1	70	1	200	0.051	0.254
32	F	0	0.5	1	75	1	200	0.058	0.291
33	F	0	0.5	1	80	1	200	0.055	0.277
34	F	0	0.5	1	85	1	200	0.053	0.267
35	F	0	0.5	1	90	1	200	0.047	0.233
30	F	1	0.5	2	30	1	150	0.038	0.192
31	F	1	0.5	2	50	1	150	0.120	0.599
36	F	1	0.5	2	70	1	200	0.044	0.219
32	F	1	0.5	2	75	1	200	0.039	0.196
33	F	1	0.5	2	80	1	200	0.043	0.216
34	F	1	0.5	2	85	1	200	0.021	0.106
35	F	1	0.5	2	90	1	200	0.023	0.113

Table 6. Position 2 FDTD results by depth from surface of the anatomical model.

Depth(mm)	30 MHz	35 MHz	40 MHz	45 MHz	50 MHz	55 MHz	70 MHz	75 MHz	80 MHz	85 MHz	90 MHz	225 MHz	275 MHz	325 MHz	400 MHz	450 MHz
0	0.017	0.015	0.013	0.012	0.011	0.010	0.010	0.010	0.010	0.011	0.012	0.042	0.037	0.039	0.044	0.041
5	0.017	0.014	0.013	0.012	0.011	0.010	0.009	0.008	0.008	0.009	0.009	0.023	0.019	0.018	0.018	0.018
10	0.057	0.049	0.044	0.040	0.036	0.033	0.027	0.027	0.027	0.028	0.029	0.073	0.051	0.042	0.041	0.038
15	0.089	0.077	0.069	0.063	0.057	0.052	0.043	0.042	0.042	0.043	0.044	0.107	0.070	0.054	0.051	0.046
20	0.128	0.112	0.101	0.093	0.085	0.078	0.065	0.063	0.062	0.061	0.062	0.144	0.089	0.060	0.051	0.046
25	0.151	0.132	0.120	0.111	0.103	0.095	0.079	0.076	0.074	0.074	0.073	0.169	0.106	0.064	0.047	0.038
30	0.137	0.122	0.112	0.105	0.097	0.090	0.076	0.073	0.071	0.070	0.069	0.156	0.103	0.059	0.036	0.025
35	0.123	0.111	0.102	0.097	0.091	0.085	0.072	0.070	0.068	0.066	0.065	0.141	0.100	0.059	0.033	0.018
40	0.115	0.104	0.097	0.093	0.087	0.082	0.072	0.069	0.067	0.066	0.064	0.129	0.099	0.062	0.035	0.018
45	0.107	0.098	0.092	0.089	0.084	0.080	0.071	0.069	0.067	0.066	0.064	0.115	0.097	0.066	0.039	0.020
50	0.082	0.076	0.072	0.070	0.067	0.064	0.058	0.056	0.055	0.054	0.052	0.081	0.074	0.055	0.034	0.018
55	0.035	0.033	0.031	0.030	0.029	0.028	0.026	0.026	0.025	0.024	0.024	0.030	0.030	0.024	0.015	0.009
60	0.009	0.009	0.009	0.009	0.008	0.008	0.008	0.008	0.008	0.007	0.007	0.008	0.007	0.006	0.004	0.002
65	0.007	0.007	0.007	0.007	0.006	0.006	0.006	0.006	0.006	0.006	0.006	0.005	0.005	0.004	0.003	0.002
70	0.013	0.013	0.012	0.012	0.012	0.012	0.011	0.011	0.011	0.011	0.010	0.006	0.007	0.007	0.006	0.004
75	0.010	0.010	0.010	0.010	0.010	0.010	0.009	0.009	0.009	0.009	0.009	0.006	0.006	0.006	0.005	0.004
80	0.005	0.005	0.005	0.005	0.005	0.005	0.004	0.004	0.004	0.005	0.005	0.003	0.003	0.003	0.002	0.001
85	0.003	0.003	0.003	0.003	0.003	0.003	0.003	0.003	0.003	0.003	0.003	0.002	0.002	0.001	0.001	0.001
90	0.003	0.003	0.003	0.003	0.003	0.003	0.003	0.004	0.004	0.004	0.004	0.002	0.002	0.001	0.001	0.001
95	0.003	0.003	0.003	0.004	0.004	0.004	0.004	0.004	0.004	0.004	0.004	0.002	0.001	0.001	0.001	0.001
100	0.003	0.003	0.003	0.003	0.004	0.004	0.004	0.004	0.004	0.004	0.004	0.002	0.001	0.001	0.001	0.001
105	0.003	0.003	0.003	0.004	0.004	0.004	0.004	0.004	0.004	0.004	0.004	0.002	0.001	0.001	0.001	0.000
110	0.004	0.004	0.004	0.004	0.004	0.005	0.005	0.005	0.005	0.005	0.005	0.002	0.002	0.001	0.001	0.001
115	0.007	0.007	0.007	0.007	0.008	0.008	0.008	0.009	0.009	0.009	0.010	0.005	0.005	0.003	0.002	0.001
120	0.028	0.029	0.033	0.031	0.032	0.033	0.037	0.039	0.040	0.042	0.044	0.028	0.027	0.019	0.015	0.011
125	0.056	0.057	0.059	0.060	0.061	0.063	0.070	0.073	0.075	0.078	0.081	0.049	0.046	0.033	0.028	0.022
130	0.050	0.050	0.049	0.052	0.053	0.054	0.060	0.062	0.064	0.067	0.069	0.041	0.041	0.031	0.028	0.023
135	0.019	0.019	0.020	0.020	0.021	0.021	0.024	0.025	0.026	0.027	0.028	0.018	0.019	0.015	0.014	0.013
140	0.006	0.006	0.006	0.006	0.006	0.006	0.007	0.007	0.008	0.008	0.008	0.005	0.005	0.004	0.003	0.003
145	0.017	0.016	0.017	0.017	0.017	0.017	0.019	0.020	0.020	0.021	0.022	0.010	0.008	0.005	0.005	0.005
160	0.006	0.006	0.006	0.006	0.006	0.006	0.007	0.007	0.008	0.008	0.009	0.006	0.006	0.005	0.005	0.005
165	0.002	0.002	0.002	0.002	0.002	0.002	0.002	0.002	0.002	0.002	0.002	0.002	0.003	0.003	0.003	0.002
170	0.003	0.002	0.002	0.002	0.002	0.002	0.002	0.002	0.002	0.002	0.002	0.002	0.002	0.002	0.002	0.002
175	0.003	0.002	0.002	0.002	0.002	0.002	0.002	0.002	0.002	0.002	0.002	0.002	0.002	0.002	0.002	0.002
180	0.002	0.002	0.002	0.002	0.002	0.002	0.002	0.002	0.002	0.002	0.002	0.002	0.002	0.002	0.002	0.002
185	0.002	0.002	0.002	0.002	0.001	0.001	0.001	0.001	0.001	0.002	0.002	0.002	0.002	0.002	0.002	0.002
190	0.002	0.001	0.001	0.001	0.001	0.001	0.001	0.001	0.001	0.001	0.001	0.002	0.002	0.002	0.003	0.002
235	0.006	0.005	0.004	0.003	0.003	0.002	0.002	0.001	0.001	0.001	0.001	0.003	0.004	0.004	0.005	0.006
240	0.030	0.023	0.018	0.015	0.013	0.011	0.007	0.007	0.006	0.005	0.005	0.005	0.005	0.004	0.006	0.007
245	0.051	0.039	0.031	0.026	0.022	0.019	0.013	0.011	0.010	0.009	0.008	0.008	0.006	0.006	0.008	0.010
250	0.023	0.017	0.014	0.012	0.010	0.009	0.006	0.005	0.005	0.004	0.004	0.007	0.007	0.009	0.012	0.012
255	0.010	0.008	0.006	0.006	0.005	0.005	0.004	0.004	0.003	0.003	0.003	0.011	0.013	0.016	0.019	0.018
260	0.011	0.009	0.007	0.006	0.006	0.005	0.004	0.004	0.004	0.004	0.004	0.010	0.012	0.014	0.016	0.015
265	0.014	0.011	0.009	0.008	0.007	0.006	0.005	0.005	0.005	0.005	0.005	0.010	0.012	0.014	0.016	0.01

Table 7. Position 1 FDTD results by depth from the surface of the back of the anatomical model.

Depth(mm)	30 MHz	35 MHz	40 MHz	45 MHz	50 MHz	55 MHz	70 MHz	75 MHz	80 MHz	85 MHz	90 MHz	225 MHz	275 MHz	325 MHz	400 MHz	450 MHz
0	0.038	0.033	0.030	0.028	0.025	0.024	0.021	0.021	0.022	0.023	0.024	0.090	0.077	0.078	0.084	0.073
5	0.036	0.031	0.027	0.025	0.023	0.021	0.017	0.017	0.017	0.018	0.018	0.047	0.033	0.029	0.031	0.026
10	0.045	0.039	0.035	0.032	0.029	0.026	0.022	0.022	0.022	0.022	0.023	0.061	0.042	0.036	0.038	0.032
15	0.113	0.098	0.088	0.081	0.074	0.068	0.057	0.055	0.055	0.055	0.056	0.144	0.095	0.070	0.064	0.051
20	0.182	0.158	0.143	0.131	0.120	0.111	0.093	0.090	0.089	0.089	0.090	0.230	0.152	0.105	0.089	0.069
25	0.164	0.144	0.131	0.122	0.113	0.105	0.088	0.085	0.084	0.083	0.083	0.209	0.143	0.093	0.067	0.048
30	0.150	0.133	0.123	0.115	0.107	0.100	0.085	0.082	0.080	0.079	0.078	0.192	0.139	0.090	0.057	0.036
35	0.136	0.123	0.114	0.108	0.101	0.095	0.082	0.079	0.077	0.076	0.075	0.174	0.136	0.092	0.056	0.032
40	0.125	0.113	0.106	0.101	0.096	0.091	0.079	0.077	0.075	0.073	0.072	0.156	0.132	0.096	0.061	0.034
45	0.115	0.106	0.100	0.096	0.092	0.087	0.077	0.075	0.073	0.072	0.070	0.138	0.125	0.099	0.068	0.040
50	0.112	0.104	0.099	0.096	0.092	0.089	0.080	0.078	0.076	0.074	0.073	0.124	0.119	0.102	0.076	0.047
55	0.067	0.062	0.059	0.058	0.056	0.053	0.048	0.047	0.046	0.045	0.044	0.068	0.069	0.061	0.049	0.032
60	0.018	0.017	0.016	0.016	0.016	0.015	0.014	0.014	0.014	0.014	0.013	0.017	0.018	0.018	0.017	0.013
65	0.019	0.018	0.018	0.018	0.017	0.017	0.016	0.016	0.016	0.016	0.015	0.017	0.018	0.019	0.018	0.015
70	0.016	0.015	0.015	0.015	0.015	0.015	0.014	0.014	0.014	0.014	0.014	0.012	0.013	0.014	0.014	0.012
75	0.010	0.009	0.009	0.009	0.009	0.009	0.009	0.009	0.009	0.009	0.009	0.006	0.007	0.007	0.007	0.006
80	0.012	0.012	0.012	0.012	0.012	0.012	0.012	0.012	0.012	0.013	0.013	0.008	0.007	0.006	0.006	0.005
85	0.008	0.008	0.009	0.009	0.009	0.009	0.009	0.009	0.009	0.009	0.009	0.005	0.004	0.003	0.003	0.003
90	0.004	0.005	0.005	0.005	0.005	0.005	0.005	0.005	0.005	0.005	0.006	0.002	0.002	0.002	0.002	0.002
95	0.004	0.005	0.005	0.005	0.005	0.005	0.005	0.005	0.006	0.006	0.006	0.002	0.002	0.002	0.002	0.001
100	0.005	0.005	0.005	0.005	0.005	0.005	0.006	0.006	0.006	0.006	0.006	0.002	0.002	0.002	0.001	0.001
105	0.006	0.006	0.006	0.007	0.007	0.007	0.007	0.008	0.008	0.008	0.008	0.003	0.002	0.002	0.002	0.001
110	0.006	0.006	0.007	0.007	0.007	0.007	0.008	0.008	0.008	0.008	0.008	0.003	0.003	0.002	0.002	0.001
115	0.007	0.007	0.007	0.007	0.007	0.007	0.008	0.008	0.008	0.009	0.009	0.004	0.003	0.003	0.002	0.001
120	0.036	0.036	0.036	0.038	0.038	0.039	0.042	0.043	0.044	0.045	0.047	0.022	0.018	0.014	0.012	0.008
125	0.037	0.037	0.037	0.038	0.039	0.040	0.043	0.044	0.045	0.046	0.048	0.022	0.018	0.015	0.012	0.009
130	0.005	0.005	0.005	0.006	0.006	0.006	0.006	0.006	0.007	0.007	0.007	0.003	0.002	0.002	0.002	0.002
135	0.004	0.004	0.004	0.004	0.004	0.004	0.004	0.004	0.004	0.004	0.005	0.002	0.002	0.001	0.001	0.001
155	0.017	0.016	0.016	0.016	0.016	0.017	0.019	0.020	0.021	0.022	0.022	0.016	0.015	0.015	0.016	0.018
160	0.001	0.001	0.001	0.001	0.001	0.001	0.001	0.001	0.001	0.001	0.001	0.001	0.001	0.001	0.001	0.001
165	0.001	0.001	0.001	0.001	0.001	0.001	0.001	0.001	0.001	0.001	0.001	0.001	0.001	0.001	0.001	0.001
170	0.002	0.002	0.002	0.002	0.002	0.002	0.002	0.002	0.002	0.002	0.002	0.001	0.002	0.001	0.001	0.001
175	0.003	0.002	0.002	0.002	0.002	0.002	0.002	0.002	0.002	0.002	0.002	0.001	0.001	0.001	0.001	0.001
180	0.003	0.002	0.002	0.002	0.002	0.002	0.001	0.001	0.001	0.001	0.001	0.001	0.001	0.001	0.001	0.001
185	0.005	0.004	0.003	0.003	0.003	0.002	0.002	0.002	0.002	0.002	0.002	0.001	0.001	0.001	0.001	0.001
190	0.007	0.005	0.004	0.004	0.003	0.003	0.003	0.002	0.002	0.002	0.002	0.001	0.001	0.001	0.001	0.001
195	0.008	0.006	0.005	0.004	0.004	0.003	0.003	0.003	0.002	0.002	0.002	0.001	0.001	0.001	0.001	0.001
200	0.008	0.006	0.005	0.004	0.004	0.003	0.003	0.002	0.002	0.002	0.002	0.001	0.001	0.001	0.000	0.001
205	0.008	0.006	0.005	0.004	0.003	0.003	0.002	0.002	0.002	0.002	0.001	0.000	0.001	0.001	0.000	0.001
210	0.007	0.005	0.004	0.003	0.003	0.002	0.002	0.001	0.001	0.001	0.001	0.000	0.000	0.000	0.000	0.001
215	0.006	0.005	0.004	0.003	0.002	0.002	0.001	0.001	0.001	0.001	0.001	0.001	0.001	0.000	0.001	0.001
220	0.005	0.004	0.003	0.003	0.002	0.002	0.001	0.001	0.001	0.001	0.001	0.001	0.001	0.001	0.001	0.001
225	0.005	0.004	0.003	0.003	0.002	0.002	0.001	0.001	0.001	0.001	0.001	0.001	0.001	0.001	0.001	0.001
230	0.014	0.011	0.009	0.007	0.006	0.005	0.003	0.003	0.003	0.002	0.002	0.002	0.002	0.002	0.003	0.003
235	0.038	0.029	0.023	0.019	0.016	0.014	0.010	0.008	0.007	0.007	0.006	0.007	0.005	0.005	0.007	0.008
240	0.020	0.015	0.012	0.010	0.009	0.008	0.005	0.005	0.004	0.004	0.003	0.005	0.004	0.005	0.007	0.006
245	0.009	0.007	0.006	0.005	0.004	0.004	0.003	0.002	0.002	0.002	0.002	0.004	0.005	0.006	0.007	0.006
250	0.011	0.008	0.007	0.006	0.005	0.004	0.003	0.003	0.003	0.002	0.002	0.004	0.005	0.006	0.007	0.006
255	0.011	0.009	0.007	0.006	0.005	0.005	0.003	0.003	0.003	0.003	0.003	0.004	0.005	0.006	0.006	0.006
260	0.019	0.015	0.013	0.011	0.010	0.009	0.007	0.006	0.006	0.006	0.005	0.008	0.007	0.008	0.009	0.008

Table 8. Position 0 FDTD results from surface of the back of the anatomical model.

Depth(mm)	30 MHz	35 MHz	40 MHz	45 MHz	50 MHz	55 MHz	70 MHz	75 MHz	80 MHz	85 MHz	90 MHz	225 MHz	275 MHz	325 MHz	400 MHz	450 MHz
0	0.108	0.096	0.087	0.081	0.075	0.070	0.061	0.060	0.061	0.064	0.067	0.234	0.201	0.204	0.221	0.193
5	0.043	0.038	0.035	0.033	0.031	0.029	0.024	0.022	0.021	0.021	0.020	0.049	0.037	0.033	0.038	0.035
10	0.043	0.038	0.034	0.032	0.029	0.027	0.022	0.022	0.021	0.022	0.022	0.056	0.041	0.035	0.038	0.031
15	0.134	0.116	0.104	0.096	0.087	0.080	0.068	0.066	0.066	0.066	0.068	0.180	0.127	0.100	0.098	0.079
20	0.212	0.184	0.167	0.154	0.141	0.130	0.109	0.106	0.105	0.106	0.107	0.283	0.200	0.151	0.138	0.112
25	0.187	0.164	0.150	0.140	0.129	0.120	0.101	0.098	0.097	0.097	0.097	0.253	0.182	0.131	0.107	0.085
30	0.158	0.140	0.129	0.122	0.113	0.106	0.091	0.088	0.086	0.085	0.085	0.218	0.165	0.118	0.086	0.064
35	0.137	0.123	0.115	0.109	0.102	0.096	0.083	0.081	0.079	0.078	0.077	0.192	0.155	0.116	0.080	0.055
40	0.122	0.111	0.105	0.100	0.095	0.090	0.079	0.077	0.075	0.074	0.073	0.171	0.148	0.118	0.085	0.057
45	0.114	0.106	0.100	0.096	0.092	0.088	0.079	0.077	0.075	0.073	0.072	0.155	0.144	0.123	0.097	0.067
50	0.104	0.097	0.093	0.091	0.087	0.084	0.076	0.074	0.073	0.071	0.070	0.134	0.132	0.120	0.103	0.075
55	0.086	0.081	0.079	0.077	0.075	0.073	0.068	0.067	0.065	0.064	0.063	0.104	0.105	0.100	0.091	0.069
60	0.044	0.042	0.041	0.040	0.039	0.038	0.036	0.036	0.035	0.035	0.034	0.050	0.052	0.052	0.049	0.039
65	0.011	0.010	0.010	0.010	0.010	0.009	0.009	0.009	0.009	0.009	0.009	0.010	0.011	0.012	0.012	0.011
70	0.013	0.012	0.012	0.012	0.012	0.011	0.011	0.010	0.010	0.010	0.010	0.010	0.011	0.013	0.013	0.012
75	0.017	0.016	0.016	0.016	0.016	0.016	0.015	0.015	0.015	0.015	0.015	0.012	0.013	0.014	0.015	0.014
80	0.016	0.016	0.016	0.015	0.015	0.015	0.015	0.015	0.015	0.015	0.015	0.010	0.011	0.012	0.013	0.012
85	0.011	0.011	0.010	0.010	0.010	0.010	0.009	0.009	0.009	0.009	0.009	0.005	0.007	0.009	0.010	0.010
90	0.006	0.006	0.005	0.005	0.005	0.005	0.005	0.005	0.005	0.005	0.005	0.003	0.004	0.006	0.007	0.007
95	0.003	0.003	0.003	0.003	0.003	0.003	0.003	0.003	0.003	0.003	0.003	0.002	0.002	0.004	0.004	0.005
100	0.003	0.003	0.003	0.003	0.003	0.003	0.003	0.003	0.003	0.003	0.003	0.002	0.002	0.003	0.003	0.004
105	0.002	0.002	0.002	0.002	0.002	0.003	0.003	0.003	0.003	0.003	0.003	0.001	0.001	0.002	0.002	0.003
110	0.002	0.002	0.002	0.002	0.002	0.002	0.002	0.002	0.003	0.003	0.003	0.001	0.001	0.002	0.002	0.002
115	0.003	0.003	0.003	0.003	0.003	0.003	0.004	0.004	0.004	0.004	0.004	0.002	0.002	0.002	0.002	0.002
120	0.022	0.022	0.025	0.023	0.023	0.023	0.025	0.026	0.026	0.027	0.028	0.014	0.012	0.011	0.009	0.006
125	0.021	0.021	0.024	0.022	0.022	0.023	0.024	0.025	0.025	0.026	0.026	0.013	0.011	0.010	0.008	0.005
130	0.003	0.003	0.003	0.003	0.003	0.003	0.003	0.003	0.003	0.003	0.003	0.002	0.002	0.002	0.002	0.001
135	0.003	0.003	0.003	0.003	0.003	0.003	0.003	0.003	0.003	0.003	0.003	0.002	0.002	0.003	0.002	0.002
155	0.005	0.005	0.005	0.005	0.005	0.005	0.006	0.006	0.006	0.006	0.006	0.004	0.005	0.005	0.004	0.004
160	0.007	0.007	0.008	0.008	0.008	0.008	0.009	0.009	0.009	0.010	0.010	0.007	0.007	0.006	0.006	0.005
165	0.019	0.015	0.012	0.010	0.008	0.007	0.005	0.004	0.004	0.003	0.003	0.001	0.001	0.002	0.003	0.004
170	0.016	0.012	0.009	0.008	0.006	0.005	0.004	0.003	0.003	0.002	0.002	0.002	0.001	0.001	0.002	0.002
175	0.019	0.015	0.012	0.010	0.008	0.007	0.004	0.004	0.003	0.003	0.002	0.003	0.002	0.002	0.003	0.003
180	0.041	0.031	0.025	0.020	0.017	0.014	0.009	0.008	0.007	0.006	0.005	0.006	0.004	0.004	0.006	0.006
185	0.035	0.027	0.021	0.017	0.015	0.012	0.008	0.007	0.006	0.005	0.004	0.005	0.003	0.004	0.006	0.006
190	0.020	0.015	0.012	0.010	0.009	0.007	0.005	0.004	0.004	0.003	0.003	0.003	0.003	0.003	0.004	0.004
195	0.022	0.017	0.014	0.011	0.010	0.008	0.006	0.005	0.005	0.004	0.004	0.004	0.003	0.004	0.005	0.005
200	0.042	0.033	0.027	0.023	0.020	0.017	0.012	0.011	0.010	0.009	0.008	0.009	0.007	0.006	0.008	0.007

Table 9. Position -1 FDTD results by depth from surface of the back of the anatomical model.

Depth(mm)	30 MHz	35 MHz	40 MHz	45 MHz	50 MHz	55 MHz	70 MHz	75 MHz	80 MHz	85 MHz	90 MHz	225 MHz	275 MHz	325 MHz	400 MHz	450 MHz
0	0.132	0.119	0.110	0.103	0.096	0.089	0.075	0.072	0.070	0.069	0.068	0.196	0.161	0.157	0.179	0.171
5	0.048	0.043	0.039	0.037	0.035	0.032	0.027	0.027	0.026	0.026	0.026	0.054	0.040	0.037	0.041	0.038
10	0.125	0.110	0.100	0.092	0.085	0.079	0.066	0.064	0.063	0.063	0.063	0.155	0.112	0.095	0.101	0.095
15	0.191	0.167	0.152	0.141	0.130	0.120	0.100	0.097	0.095	0.095	0.095	0.237	0.169	0.134	0.132	0.123
20	0.207	0.183	0.167	0.155	0.144	0.133	0.112	0.109	0.107	0.106	0.106	0.264	0.191	0.145	0.129	0.115
25	0.199	0.177	0.163	0.153	0.142	0.132	0.113	0.109	0.107	0.106	0.105	0.261	0.197	0.148	0.119	0.101
30	0.179	0.161	0.149	0.141	0.132	0.124	0.106	0.103	0.101	0.099	0.098	0.241	0.192	0.148	0.114	0.091
35	0.160	0.145	0.136	0.129	0.122	0.115	0.100	0.097	0.095	0.093	0.092	0.220	0.186	0.151	0.118	0.092
40	0.145	0.132	0.125	0.120	0.113	0.108	0.095	0.093	0.090	0.089	0.088	0.200	0.179	0.152	0.126	0.098
45	0.099	0.092	0.087	0.084	0.080	0.077	0.068	0.067	0.065	0.064	0.063	0.134	0.126	0.112	0.098	0.076
50	0.052	0.049	0.047	0.046	0.044	0.043	0.039	0.038	0.037	0.037	0.036	0.068	0.068	0.063	0.061	0.049
55	0.040	0.038	0.036	0.035	0.034	0.033	0.031	0.030	0.029	0.029	0.029	0.047	0.050	0.049	0.050	0.043
60	0.029	0.027	0.025	0.024	0.023	0.022	0.020	0.020	0.019	0.019	0.019	0.029	0.032	0.034	0.036	0.033
65	0.021	0.019	0.018	0.017	0.016	0.016	0.014	0.014	0.014	0.014	0.014	0.019	0.022	0.025	0.027	0.026
70	0.013	0.012	0.011	0.011	0.011	0.010	0.010	0.010	0.010	0.010	0.010	0.012	0.014	0.016	0.018	0.018
75	0.015	0.014	0.014	0.014	0.013	0.013	0.013	0.013	0.012	0.012	0.012	0.010	0.012	0.013	0.015	0.016
80	0.014	0.014	0.014	0.013	0.013	0.013	0.013	0.012	0.012	0.012	0.012	0.008	0.009	0.010	0.012	0.013
85	0.007	0.006	0.006	0.006	0.006	0.006	0.006	0.006	0.006	0.006	0.006	0.003	0.003	0.004	0.004	0.005
90	0.004	0.004	0.004	0.004	0.004	0.004	0.004	0.004	0.004	0.004	0.004	0.002	0.002	0.002	0.002	0.003
95	0.004	0.004	0.004	0.004	0.004	0.004	0.004	0.004	0.004	0.004	0.004	0.002	0.002	0.002	0.002	0.002
100	0.004	0.004	0.004	0.004	0.004	0.004	0.004	0.004	0.004	0.004	0.004	0.002	0.002	0.002	0.001	0.002
105	0.003	0.003	0.003	0.003	0.003	0.003	0.004	0.004	0.004	0.004	0.004	0.002	0.002	0.001	0.001	0.001
110	0.003	0.003	0.003	0.004	0.004	0.004	0.004	0.004	0.004	0.004	0.004	0.002	0.001	0.002	0.001	0.001
115	0.005	0.005	0.004	0.005	0.005	0.005	0.005	0.005	0.006	0.006	0.006	0.003	0.003	0.003	0.002	0.001
120	0.008	0.008	0.008	0.008	0.008	0.008	0.009	0.009	0.009	0.010	0.010	0.005	0.004	0.004	0.002	0.001
125	0.011	0.011	0.012	0.012	0.012	0.012	0.012	0.013	0.013	0.013	0.013	0.007	0.004	0.004	0.002	0.001
130	0.012	0.012	0.013	0.012	0.012	0.012	0.013	0.013	0.013	0.014	0.014	0.007	0.004	0.004	0.003	0.001
135	0.006	0.006	0.006	0.006	0.006	0.006	0.006	0.006	0.006	0.007	0.007	0.003	0.002	0.002	0.002	0.001
155	0.006	0.006	0.005	0.005	0.005	0.005	0.005	0.005	0.006	0.006	0.006	0.003	0.003	0.003	0.002	0.002
160	0.005	0.005	0.005	0.005	0.005	0.005	0.005	0.005	0.005	0.005	0.006	0.004	0.004	0.004	0.004	0.003
165	0.016	0.013	0.012	0.011	0.011	0.010	0.010	0.010	0.010	0.010	0.010	0.005	0.007	0.007	0.007	0.008
170	0.010	0.009	0.008	0.007	0.007	0.006	0.006	0.006	0.006	0.006	0.006	0.003	0.003	0.003	0.003	0.004
175	0.010	0.009	0.008	0.007	0.006	0.006	0.006	0.006	0.006	0.006	0.005	0.002	0.002	0.002	0.003	0.004
180	0.009	0.008	0.007	0.006	0.006	0.005	0.005	0.005	0.005	0.005	0.005	0.002	0.002	0.002	0.002	0.003
185	0.008	0.007	0.006	0.005	0.005	0.004	0.004	0.004	0.004	0.004	0.004	0.001	0.001	0.001	0.001	0.002
190	0.008	0.006	0.006	0.005	0.005	0.004	0.004	0.004	0.004	0.004	0.003	0.001	0.001	0.001	0.001	0.002
195	0.013	0.010	0.008	0.007	0.006	0.006	0.005	0.005	0.004	0.004	0.004	0.001	0.001	0.001	0.002	0.003
200	0.006	0.005	0.004	0.003	0.003	0.002	0.002	0.001	0.001	0.001	0.001	0.001	0.001	0.001	0.002	0.002
205	0.015	0.011	0.009	0.007	0.006	0.005	0.003	0.003	0.003	0.002	0.002	0.004	0.003	0.004	0.005	0.006
210	0.022	0.016	0.013	0.011	0.009	0.008	0.005	0.004	0.004	0.003	0.003	0.007	0.006	0.006	0.008	0.008
215	0.021	0.016	0.013	0.011	0.009	0.008	0.006	0.005	0.004	0.004	0.003	0.007	0.006	0.006	0.007	0.007

Table 10. Summary of vest antenna FDTD results. A 5mm model of the visible man (105 kg) was dressed in a model of the COMWIN Body-Borne (vest) antenna. Care was taken to make sure that there was no direct contact between the man and the vest. The basic antenna design uses cylindrical strips of perfect electrical conductor, however the front of the vest was truncated with flat portions of perfect electrical conductor to more closely duplicate the close proximity of the vest to the torso in actual field situations.

	Max SAR (W/kg) per 5 W in				
f (kHz)	1/8 g	1 g av.	10 g av.	WBA	Z_{in} (Ohms)
30	7.6	6.5	2.4	0.051	4.4+40j
35	6.8	5.9	2.2	0.048	10+52j
40	6.4	5.5	2.0	0.046	24+66j
45	6.0	5.2	1.9	0.045	51+76j
50	5.7	4.9	1.8	0.044	89+59j
55	5.4	4.7	1.8	0.044	97+16j
70	4.6	4.0	1.6	0.043	44-11j
75	4.4	3.8	1.6	0.043	35-6.6j
80	4.2	3.7	1.5	0.043	30-2.1j
85	4.0	3.6	1.5	0.043	27+2.3j
90	4.0	3.4	1.5	0.044	24+6.5j
225	5.5	2.9	1.6	0.042	47+74j
275	6.8	2.2	1.1	0.040	74+74j
325	8.5	2.2	1.3	0.039	86+62j
400	11	2.7	1.7	0.038	89+57j
450	12	2.7	1.9	0.038	86+54j